POST-PRINT https://www.sciencedirect.com/science/article/pii/S2212095515000243
Urban Climate, Volume 13, September 2015, Pages 73-93

Elsevier Editorial System(tm) for URBAN CLIMATE
Manuscript Draft

Manuscript Number: UCLIM-D-14-00132R1

Title: Breathability of compact cities

Article Type: Research Paper

Keywords: city breathability, compact cities; mean age of air; exchange velocity; wind tunnel measurements, CFD simulations

Corresponding Author: Dr. Riccardo Buccolieri, Ph.D.

Corresponding Author's Institution: University of Salento

First Author: Riccardo Buccolieri, Ph.D.

Order of Authors: Riccardo Buccolieri, Ph.D.; Pietro Salizzoni; Lionel Soulhac; Valeria Garbero; Silvana Di Sabatino

Abstract: Breathability in dense building arrays with packing densities similar to those of typical European cities is investigated using laboratory measurements and numerical simulations. We focus on arrays made up by regularly spaced square buildings forming a network of streets with right-angle intersections. It is shown that breathability can be evaluated using building ventilation concepts (mean flow rate and age of air) and from vertical mean and turbulent fluxes quantifiable through a bulk exchange velocity. Mean age of air reveals that varying wind angles result in different ventilation, which we explain through mean flow streamlines and exchange velocity. For low wind angles (wind direction almost parallel to the axes of half of the streets of the network), vertical transfer and mean transversal transfers are at minimum and removal of pollutants is associated to mean longitudinal fluxes. Larger wind angles result in better ventilation due to an increase of transversal fluxes and vertical exchange. The latter, for which a formulation is derived, shows a non-negligible contribution of the mean flow which increases with increasing wind angle. Ventilation conditions can be further altered by small differences in the array geometry. These observations are useful for the development of simple urban dispersion models.

Suggested Reviewers:

Opposed Reviewers:

Response to Reviewers:

Abstract

Breathability in dense building arrays with packing densities similar to those of typical European cities is investigated using laboratory measurements and numerical simulations. We focus on arrays made up by regularly spaced square buildings forming a network of streets with right-angle intersections. It is shown that breathability can be evaluated using building ventilation concepts (mean flow rate and age of air) and from vertical mean and turbulent fluxes quantifiable through a bulk exchange velocity. Mean age of air reveals that varying wind angles result in different ventilation, which we explain through mean flow streamlines and exchange velocity. For low wind angles (wind direction almost parallel to the axes of half of the streets of the network), vertical transfer and mean transversal transfers are at minimum and removal of pollutants is associated to mean longitudinal fluxes. Larger wind angles result in better ventilation due to an increase of transversal fluxes and vertical exchange. The latter, for which a formulation is derived, shows a non-negligible contribution of the mean flow which increases with increasing wind angle. Ventilation conditions can be further altered by small differences in the array geometry. These observations are useful for the development of simple urban dispersion models.

Keywords: city breathability*,* compact cities; mean age of air; exchange velocity; wind tunnel measurements, CFD simulations

1. Introduction

In recent years, health risks associated with microclimate variations and exposure to concentrations of harmful pollutants in cities have inspired a large number of studies focusing on the mechanisms that drive momentum, mass and heat transfer within urban canopies. According to recent studies (e.g. Fernando et al., 2010; Dallman et al., 2013; Zaijc et al., 2015) at the core of these studies there is the relationship between turbulent transfers of both active and inactive variables and urban morphology in real atmospheric conditions. Given the high complexity of the problem, often the interpretation of field measurements are backed up by numerical simulations and controlled laboratory experiments. The choice of the modelling approach depends somewhat upon the level of details of the atmospheric processes represented and therefore upon the chosen spatial scales, namely the street, the neighbourhood and the city scale (Britter and Hanna, 2003).

At the street and neighbourhood scale, experiments and numerical simulations have been carried out to evaluate the effect of a wide range of features affecting pollutant dispersion. These include the street aspect ratios, the roof-shape, the length of the canyon, the building packing density, the wind direction, etc. (e.g. Yim et al., 2009; Gousseau et al., 2011; Salim et al., 2011).

For recent reviews on these topics the reader is referred to Di Sabatino et al. (2013) and Tominaga and Stathopoulos (2013).

At the neighbourhood scale, most of the studies on pollutant dispersion focus on the case of obstacle arrays with low obstacle density (e.g. Yee and Biltoft, 2004; Coceal et al., 2007) in which wakes developing downwind of each obstacle interact with each other (Oke, 1998). The geometry of low density obstacle arrays is similar to that of North American or European suburban neighbourhoods (Di Sabatino et al., 2010). In contrast, these configurations are very different from central neighbourhoods of most European cities (Fig. 1), where buildings are regularly and densely packed. Flow and dispersion within these densely packed neighbourhoods have been rarely studied (e.g. Garbero et al., 2010; Hang et al., 2012a; Panagiotou et al., 2013) even though they are characterized by high traffic levels and a high density of population.

The main objective of the paper is to examine city breathability and consequently dispersion conditions within European-like urban canopies, focusing on the influence of a varying wind direction and of slight modifications of the geometrical parameters of the building arrays. To that purpose, we adopt concepts and terminology that were originally introduced in building ventilation analyses (Etheridge and Sandberg, 1996), a practice that is becoming customary in the field of the urban fluid mechanics. City breathability reflects the potential of a city to be ventilated under the action of the wind blowing through it. Therefore, this potential is directly related to the air flow patterns taking place within the urban canopy and resulting from the interaction between the approaching (to city) atmospheric flow with the building blocks (Panagiotou et al., 2013). The evaluation of the breathability of a city (or part of it), can be done through the estimation of bulk flow parameters such as the mean flow rate, the mean age of air and the exchange velocity. The combined analysis of mean flow rate and mean age of air allowed Buccolieri et al. (2010) and Hang et al. (2012a, 2012b) to successfully assess the breathability of urban canyons and obstacle arrays. In particular, the mean age of air was employed to directly link the rate of removal of the contaminant to the position within the urban canopy, and therefore allows for a detailed mapping of the "breathability" potential of a given neighbourhood or building configuration (Buccolieri et al., 2010; Panagiotou et al., 2013; Neophytou et al., 2014).

Other authors have attempted to quantify ventilation conditions of street canyons (e.g. Solazzo and Britter, 2007; Solazzo et al. 2010; Salizzoni et al., 2009; Moonen et al., 2011) and urban canopies (Panagiotou et al., 2013) by estimating a pollutant exchange velocity, a bulk quantity that includes all contribution to the vertical transfer of mass out of the canyon through the canopy interface. Simplified models for the exchange velocity have been proposed by Bentham and Britter (2003) who considered a constant flow velocity within the canopy layer instead of the usual logarithmic profile, and by Soulhac et al. (2013) who explicitly considered the shear layer developing at the roof level. Both parameterizations have been tested with satisfactory results within street network dispersion models simulating pollutant transfer within and above urban canopies (e.g. Hamlyn and Britter, 2005; Carpentieri et al., 2012; Ben Salem et al., 2015).

Following these authors, we investigate city breathability within European-like urban canopies (Section 2), focusing on the extreme cases of densely packed arrays and variable incident wind direction. To this aim we use Computational Fluid Dynamics (CFD) simulations (Section 3), validated against wind tunnel data (Section 4), to study the effect of wind direction and minor modification of the geometry of the array on three parameters - the mean flow rate (Section 5), the mean age of air and the exchange velocity (Section 6). Results are discussed in terms of reliability of the two main strategies adopted nowadays for the operational modelling of pollutant dispersion in city neighbourhood: canopy models (Coceal and Belcher, 2004; Di Sabatino et al. 2008; Di Sabatino et al., 2011b), which adopt a horizontally spatially-averaged description of flow and dispersion that model the obstacle array by means of morphometric parameters, such as the planar area (λ_p) and the frontal area (λ_f) indices (or the drag coefficient C_D), and street network models, which adopt explicit parameterisations for the main exchange phenomena within the urban canopy (Soulhac et al, 2011).

Fig. 1 about here

2. Description of the building configurations

Urban geometries chosen here, although still idealized, are representative of the neighbourhood scale of many European cities, with an average building height H of 12–20m and λ_p equal to around 0.40. In these urban geometries (Fig. 1), buildings are densely packed and their width exceeds that of the streets separating them. Below roof level, the interaction between the flow developing in different regions of the domain is limited and it is therefore possible to distinguish features of the flow within a street from that developing at an intersection or within a square. For these reasons, these urban geometries have been referred to as 'street networks' (Soulhac et al., 2011), since they can be properly modelled as a network of connected boxes.

The building configurations used in this study are those presented by Garbero et al. (2010), who performed wind tunnel experiments of pollutant dispersion within obstacle arrays mimicking the large scale geometry of a typical real urban area similar to those shown in Fig. 1. The physical model represents explicitly the geometrical features of the buildings by means of regular spaced blocks. In the experiments, the blocks were squares of side $L=W=250$mm in the horizontal plane and $H=50$mm high, representing 20m high buildings at a 1:400 scale.

Fig. 2 shows the three configurations studied, referred to as Configuration 1, Configuration 2 and Configuration 3. The three configurations were obtained by varying the spacing S_x and S_y between the buildings. It is worth mentioning that Configuration 3 is the same as Configuration 2 rotated by an angle of 90°. Flow and dispersion were studied for different wind directions (θ) with respect to the x-direction axis, namely 2.5°, 12.5°, 27.5° and 47.5°. The pollutant source was placed at height $H/2$ (25mm at wind tunnel scale) within an intersection located in the middle of the model.

The planar area index λ_p is equal to 0.69 for Configuration 1 and 0.59 for Configuration 2 and 3 and is independent from wind direction. The values of the frontal area index λ_f depend on the wind direction and were calculated by projecting the frontal areas of the buildings along the wind direction (Ratti et al., 2006), see Table 1.

Fig. 2 about here

Table 1 about here

In the experiments the wind tunnel floor was completely covered by blocks, in order to reproduce a well developed boundary layer flow above the simulated canopy in the terminal part of the test section, where dispersion experiments were carried. Profiles of the mean longitudinal velocity and of the turbulent kinetic energy measured in the overlying boundary layer flow are shown in Fig. 3. The neutrally stratified boundary layer depth was $\delta=15H$, with a reference undisturbed velocity $U_{ref}=4.8\text{ms}^{-1}$ at $z=\delta$.

Fig. 3 about here

3. Numerical modelling set-up

CFD simulations were performed by means of the code Fluent (2006) solving the 3D steady-state, incompressible and isothermal Reynolds-Avergaed Navier-Stokes (RANS) with the standard k-ε closure model (Launder and Spalding, 1974). The limitations of RANS closure models in simulating turbulent mass exchange phenomena in complex geometries are well documented in the literature (e.g. Tominaga and Stathopoulos, 2013). Broadly speaking, these are related to the uncertainty associated to the values of the turbulent Schmidt number Sc_t and to their inherent inability to simulating intermittent phenomena.

Despite these limitations, accurate comparisons of RANS simulations with experiments and Large Eddy Simulation (LES) have shown the reliability of the RANS models in reproducing the spatial distribution of mean velocity and concentration fields (e.g. Santiago and Martilli, 2010; Dejoan et al., 2010; Tominaga and Stathopoulos, 2013). For these reasons, RANS closure models are still widely used to investigate the main feature charactering the mechanics of ventilation of street canyons and urban canopies, as recently done in the comprehensive MUST CFD-evaluation exercise within COST Action 732 (Di Sabatino et al., 2011a). Further examples of RANS simulations are provided by Solazzo and Britter (2007) and Murena et al. (2011), who estimated the vertical exchanges within a square section and a deep street canyon, respectively. Santiago et al. (2014) studied the effects of thermal fluxes on the air circulation within a street canyon. Santiago et al. (2008) investigated the flow within and above a sparse canopy. Buccolieri et al. (2010), Hang et al. (2012a), Panagiotou et al. (2013) used RANS model to investigate the ventilation condition of urban canopies with varying packing density.

In the present study, before using RANS simulations to assess ventilation conditions within the canopy, we accurately verified the accuracy of the predicted mean concentration by a comparison with wind tunnel data. The main goal of these comparisons was to identify the values of the Schmidt number Sc_t allowing for the best agreement between simulated and measured concentrations.

Following the state-of-art simulation requirements (Di Sabatino et al., 2011a), the computational domain was built using hexahedral elements (about four millions), with a finer resolution within the entire building area (the expansion ratio between two consecutive cells was below 1.3). The smallest dimensions of the elements in the x, y and z directions were $\Delta x_{min}=\Delta y_{min}=0.1H$ and $\Delta z_{min}=0.03H$, respectively. The influence of the grid size was verified using two additional meshes (mesh 1: $\Delta x_{min}=\Delta y_{min}=0.1$H and $\Delta z_{min}=0.03$H; mesh 2: $\Delta x_{min}=\Delta y_{min}=0.1$H and $\Delta z_{min}=0.02$H). The differences of the mass fluxes entering and leaving the array computed adopting the three meshes showed difference of less than 5%. Symmetry boundary conditions, required to enforce a parallel flow, were imposed on the top and lateral sides of the domain. At the downwind boundary of the domain a pressure-outlet condition was used. No-slip wall boundary conditions were used at all solid surfaces (Fig. 4). Second order discretisation scheme was used for pressure whereas second order upwinding discretisation schemes (Barth and Jespersen, 1989) were used for mean momentum, turbulent kinetic energy, its dissipation rate and the scalar concentration in order to increase the accuracy and reduce numerical diffusion. The SIMPLE scheme was used for the pressure-velocity coupling. Simulations were run until the residuals became constant (equal or below 1e-05).

As inlet boundary conditions (see Fig. 3) we imposed profiles fitting the experimental data of mean longitudinal velocity (U), turbulent kinetic energy (k) and dissipation rate (ε). This latter quantity is estimated from direct estimates of k production term $P = -\overline{u'w'}\dfrac{dU}{dz}$ (being $\overline{u'w'}$ the Reynolds stress) and under the assumption of local equilibrium, i.e. P=ε.

The inlet wind velocity was assumed to follow a power law profile of the form:

$$\frac{U}{U_H} = \left(\frac{z}{\delta}\right)^{\alpha} \tag{1}$$

where the coefficient α=0.27 was set by fitting the experimental profile. The vertical profiles of turbulent kinetic energy (k) dissipation rate (ε) are of the form:

$$\frac{k}{u_*^{\,2}} = \frac{1}{\sqrt{C_\mu}}\left(1 - \frac{z}{\delta}\right) \tag{2}$$

$$\frac{\varepsilon\delta}{u_*^{\,3}} = \frac{\delta}{\kappa z}\left(1 - \frac{z}{\delta}\right) \tag{3}$$

where $\kappa=0.4$ the von Kàrmàn constant, C_μ=0.09 and u_*=0.23ms^{-1} is the friction velocity estimated from the Reynolds stress profiles in the wind tunnel experiments (Garbero et al., 2010).

Fig. 4 about here

Sensitivity to the inlet profiles was assessed through several tests. Values of the coefficient α and, accordingly, of the maximal k and ε levels, were varied of ± 20%. Results show that the flow tends to reach an equilibrium conditions two rows of blocks downstream the beginning of the array, irrespective to the variations imposed at the inlet profiles. As a consequence, the estimates of the mass and air fluxes leaving and entering the array do not show significant differences (less than 5%) produced by the variations of the inlet boundary conditions.

Two different types of sources were considered in the passive scalar dispersion simulations. Firstly we simulated the emission from a localized source represented by a cube of 0.02H size placed within an intersection at $z=H/2$ (as in the experiments) and after the fifth row of blocks (Fig. 2). Results achieved with this set-up are presented in Section 4 with the aim of validating CFD simulations against wind tunnel experiments. Secondly, we considered the case of a volume source, distributed uniformly over the whole volume of the canyons and intersections composing the simulated urban canopy. Results achieved with this set-up are presented in Sections 5-6 with the aim of quantifying the ventilation conditions.

The passive scalar dispersion simulations were carried out using the advection-diffusion module and testing three different values of the turbulent Schmidt number Sc_t, which was set equal to 0.3, 0.7 and 1. The analysis of the results showed that simulations results obtained with Sc_t=0.7 (standard value in Fluent) provided by far the best accordance with experimental results (see Section 4).

4. Numerical modelling validation

As a first step, we present a comparison between numerical and experimental results of Garbero et al. (2010) to demonstrate the reliability of RANS modelling to properly simulate processes that drive pollutant dispersion within the arrays. We focus first on the dispersion of a passive scalar emitted by a point source (placed at a street intersection within the canopy). As an example, Figs. 5-7 show horizontal profiles within the canopy of the longitudinal (u, x-velocity) and transversal (v, y-velocity) components of the mean velocity normalized by U_H=1.6ms^{-1} (the undisturbed x-velocity component of the approaching flow at the building height H (Figs. 5-6)). Fig. 7 shows profiles at different locations of the mean pollutant concentration c expressed in non-dimensional form as:

$$c^+ = {cU_H HL}/{Q} \tag{4}$$

where Q is the emission rate (gs^{-1}). In all figures the origin of the x-y coordinate system is located at the source position (see Fig. 2).

In particular, Fig. 5 shows numerical and experimental horizontal and vertical profiles of the mean velocity for Configurations 1 and 2 (θ=2.5°). We observe that u is much larger than v. This is due to the channelling effect in the street whose axis is (almost) aligned with the wind direction and the weak interaction with the flow within the transversal streets. This is confirmed by the low values of w, which indicates that mean vertical transfers are small compared to those in the longitudinal direction. This flow structure is altered for larger wind directions (Fig. 6), where u and v at the street intersections are of the same magnitude, suggesting the presence of a higher interaction of the flows coming from (or directed to) the streets forming the intersections.

The main differences between the experimental and numerical results are observed within the street intersection (Figs. 5-6), which represents the region where the streamlines are more complex (Soulhac et al., 2009). This will be discussed in detail in Section 5.

Fig. 5 about here

Fig. 6 about here

Despite local differences between numerical and experimental results observed in the velocity field, the concentration fields provided by the numerical simulation reproduce generally well those observed experimentally (Fig. 7). The concentration profiles for θ=2.5° clearly reflect what evidenced in Fig. 5, i.e. that the channeling of the flow confines the plume within the street in which the pollutant has been emitted and that its spread in the lateral streets is inhibited by the absence of a mean lateral advection. This channelling takes place for both Configurations 1 and 2, and is therefore almost insensitive to S_y/H (see Fig. 7a,b). Conversely, a larger ratio S_x/H (Fig. 7c) results in completely different concentration patterns. In this case, as shown by Hoydysh and Dabberdt (1994), even a slight asymmetry in the flow configuration, as that occurring for θ=2.5°, produces enhanced lateral fluxes at street intersection and much higher concentration level in the lateral streets. However, since the mean velocity component along the lateral street is lower than the intensity of the vertical transfer, from the street to the outer atmosphere, the concentration within the lateral streets exhibits a high gradient along the *y*-direction.

The role of these lateral fluxes at street intersections and of those along the street axes is significantly increased for larger incident angles (Fig. 7d). Their combined effect enhances the effectiveness of the transfer of momentum in the horizontal plane compared to that in the vertical direction. In this case the concentration pattern within the array is characterized by approximately constant values within the street and sharp gradient at the intersections. Physically, this witnesses a much more efficient transfer within the street compared to that at street intersections and at roof level, as will be discussed in detail in Section 6. The intensity of this latter transfer plays evidently a major role in the ventilation of the canopy, and we expect it to depend on both the street geometry and the wind direction.

Fig. 7 about here

To assess the overall model performance, several standard metrics have been applied to the concentration values measured and calculated at both z=H/2 and z=2H, namely the normalized mean square error NMSE, the fraction of predictions within a factor of two of observations FAC2, the fractional bias FB = FB_{fn} (false negative) – FB_{fb} (false positive) and the Hit Rate validation test q (using a fractional deviation equal to 0.25 and an absolute deviation equal to 0.04 based on experimental uncertainty). According to COST Action 732 (Di Sabatino et al., 2011a), even though there are not fixed values, recommended criteria may be given by the following values: NMSE ≤ 1.5; FAC2 ≥ 0.5; −0.3 ≤ FB ≤ 0.3; q≥0.66. Results are presented in Table 2, which shows a quite satisfactory model performance in terms of the essential features of the mean velocity and concentration field, even though the Hit Rate is slightly below the limit value. Further it should be noted that the FB shows a slight tendency of the model in underestimating the experimental concentration, which occurs evenly for any configuration studied. Therefore this implies a systematic minor overestimation of all ventilation conditions presented here, as estimated by the CFD models. This supports the use of the RANS approach to investigate city breathability, as reported in the next sections.

Table 2 about here

5. Air flow within the arrays

Once validated against experiments, numerical modelling is used as a tool to enlighten features of the flow that would require a big experimental effort to be estimated, such as the air and mass fluxes entering and leaving the obstacle array, and that are meaningful for ventilation analyses. As suggested from the analysis of the mean concentration presented in Section 4, mass transfers are sensitive to the geometrical configurations and wind direction. This dependence may alter significantly the ventilation condition within the array. Our aim here is to gain further information on these transfer processes by applying breathability concepts to CFD results.

5.1. Flow pattern

The sketch of streamlines (Fig. 8), coloured depending on the local value of w/U_H, illustrates the flow structure while highliting the effect of the street aspect ratio and the wind direction. The streamlines start from two vertical planes yz (i.e. almost perpendicular to the wind when θ=2.5°) located in the first two parallel street canyons at the left of each subfigure. We first focus on the θ=2.5° case (Fig. 8a,b). For S_x=H (Configurations 1-2) interactions between the flow within the intersection and the flow within the crossing streets are reduced. The flow is characterized by a channelling along the main street parallel to the wind direction and vertical axes vortices forming in the crossing streets close to the street intersections. Values of w/U_H are low, suggesting a minor impact of vertical transfer. Conversely, for S_x=2H (Configuration 3) vortices at the intersections interact much more with the street flow leading to complex flow patterns that are strongly coupled with the flow above. Despite the low porosity of the obstacle array (λ_p=0.59), the flow shows similar features to those commonly observed in the wake interference regime (Oke, 1988).

For increasing wind directions, the organized structure of the flow observed for Configuration 1 and 2 progressively disappears and the streamlines coming from the streets merge within the street intersections. A flow channelling along the street axes is observed both along the x and y directions and vortices found behind the buildings in the low θ case disappear. As the wind direction attains θ=47.5° (Fig. 8c,d), the street aspect ratio seems to loose its influence on the overall flow structure and the flow observed in the two Configuration 1 and Configuration 3 (that is similar to Configuration 2 for θ=47.5°) becomes very similar. Finally, it is to note that the values of w/U_H are locally larger (especially at street intersections) than those observed for lower wind angles. As discussed in Section 6, this feature has a direct impact on the magnitude of the vertical fluxes of pollutant out of the canopy.

Fig. 8 about here

5.2. Mean flow rate

A current methodology for the evaluation of the efficiency of forced and naturally ventilation of enclosed spaces rely on the estimate of the mean air flow rates leaving and entering a control volume (Etheridge and Sandberg, 1996). Following Buccolieri et al. (2010), we have adapted this concept, originally used for confined domains, to the case of a semi-confined domain, as the air volumes within the obstacle array. To that purpose we define a normalized flow rate as:

$$q^* = q \big/ q_{ref} = \int_A \overline{U}_i \cdot n_i dA \Bigg/ \int_{A_{ref}} \overline{u}_{ref} \cdot n dA_{ref} \tag{5}$$

where $\overline{U}_i$ is the spatially-averaged velocity over the area (A) of the street opening (which corresponds to the empty space between two adjacent buildings; alternatively, upstream, downstream, sides and top roof of the array) and n_i is the normal direction of street openings. q_{ref} is the reference flow rate through the area A_{ref} far upstream of the building array, where the wind velocity is $\overline{u}_{ref}$ (along the x-direction, see Fig. 2). The extent of the reference area A_{ref} is the same as that of the section of the street through which air enters within the array. The flow rates are defined positive (red in the colour figure, black in the B&W figure) for air entering the array, negative (yellow in the colour figure, grey in the B&W figure) for air leaving the array. The vertical flow rate is indicated by an arrow at the centre of each array.

For θ=2.5° and θ=12.5° (Fig. 9a,b) the flow enters the array from the lateral sides (positive flow rates) for all three configurations. This is in accordance with results of Buccolieri et al. (2010) for regular arrays of cubes with similar λ_p and a perpendicular approaching flow. However, the direction of the vertical net air flow of Configuration 2 differs from that of the two other configurations. The vertical flow rate for Configuration 3 - θ=2.5° is much larger than that in any of the other configurations, which is evidently linked to the pattern of the streamlines shown in Fig. 8b. When the angle θ is slightly increased (=12.5°) the vertical flow is significantly reduced, almost by a factor 2, but it is still larger than that observed in the other configurations. The lowest values of the mean vertical flow rate are observed, in all configurations, for θ=27.5°. Obviously, this does not necessarily mean that there are no vertical fluxes, but only that their net contribution is almost null.

It is worth noting that we cannot identify clear tendencies of the intensity of mean air flows both as a function of the array geometry and the wind direction. Therefore, we have to conclude that the sole analysis of this parameter does not allow us to quantify the ventilation conditions of the simulated city neighbourhood.

Fig. 9 about here

6. Pollutant dispersion and ventilation analyses

To assess and to identify the mechanisms that control city breathability, we estimated two parameters: the mean age of air and the bulk vertical exchange velocity. To that purpose we apply the homogeneous emission method (Hang et al., 2009), which is based on the analysis of numerical experiments of pollutant dispersion emitted by a uniformly distributed emission rate within the array (see Section 3).

6.1. Mean age of air

The mean age of air is the typical time for the mass of a pollutant within an arbitrary small control volume to be washed-out of an airflow system. From a Lagrangian point of view, it can be interpreted as a measure of the average time that a parcel of air takes to reach an arbitrary point after entering in an airflow system or to be removed out of it (Etheridge and Sandberg, 1996). The lower the local mean age of air, the larger the local ventilation will be. Given the effective uniformly distributed emission rate Q_U per unit volume and the corresponding tracer concentration field c at a given location, the local mean age of air $\tau = c/Q_U$ is normalized as:

$$\tau^* = \tau q_{ref} \big/ VOL \tag{6}$$

where q_{ref} is the reference flow rate as defined in Eq. (5), VOL is the volume of the gaps within the building array from the ground to the pedestrian level, that in our cases corresponds to 0.1H (2m in full scale) and it is at the fourth cell above the ground.

In their previous work, Buccolieri et al. (2010) showed the link between urban ventilation and the building packing density, expressed in terms of the planar area index λ_p. Their findings for regular arrays of cubes (i.e. $\lambda_p = \lambda_f$) subjected to a perpendicular approaching flow, show that the mean age of air increases as packing density increases. In particular, maximum values of mean age of air occurred for λ_p =0.56 due to the presence of smaller recirculation zones with lower wind velocity and larger pollutant accumulation. Pushing their analysis further, here the focus is to consider the case of densely packed arrays with similar λ_p and slight variations in λ_f which corresponds to varying incident wind directions.

Table 3 shows the maximum, the spatial average and the standard deviation of the normalized mean age of air values at pedestrian level, whereas Fig. 10 shows the normalized mean age of air at pedestrian level. In all the cases investigated, maximum and mean values of the age of air decrease (up to about 50%) as the deviation of wind direction from being perpendicular increases.

The worst ventilation conditions occur for low incident angles (Fig. 10a,b) and it is observed for Configuration 2 - θ=2.5°. This can be due to an accumulation of pollutant related to the mean advection within the street, which makes the mean age of air older in downstream regions, especially for a wind direction parallel to the street axis for which the mean advection intensity is maximized. As discussed by Soulhac and Salizzoni (2010), this accumulation may determine ground level concentrations that can even exceed those observed with a perpendicular wind direction that is often erroneously identified as the worst case for street ventilation. These reduced ventilation in Configuration 2 persists for increasing θ, up to θ=27.5°. The wind direction θ=27.5° turns out to be critical also for Configurations 1 and 3 (Fig. 10c,d), producing the highest maximum and averaged mean age of air.

Table 3 about here

This picture of the flow and dispersion is completely altered in Configuration 3, which experiences the best ventilation conditions for low incident angles also (θ=2.5° and θ=12.5°). This is due to the combined effect of an efficient vertical exchange (see Subsection 6.2), which is related to the intense vertical mean flows (Subsection 5.1) and relative low advective fluxes along the street axes, which preclude the accumulation of pollutant within the street previously described.

Fig. 10 about here

In summary, the value of the mean age of air shows an important variability both in maximum values and in spatially-averaged values. This variability is due to changing wind directions and to slight variations in the array geometry, which in turn induces little variations in the morphometric parameters λ_p and λ_f. We stress here that all these features could not be easily inferred from the sole analysis of the mean air flow rates showing the challenge in defining different independent parameters to asses city breathability.

These findings have important implications for the operational modelling of pollutant dispersion in such dense packed urban geometries. The fact that the ventilation conditions cannot be easily linked to the variation of simple morphometric parameters implies indeed evident shortcomings for the adoption of modified Gaussian models, as those discussed by Huq and Franzese (2013) and Venkatram et al. (2004) and of canopy models (e.g. Di Sabatino et al., 2011b) that aim in describing the spatially-averaged ventilation conditions based on a reduced set of parameters. The operational modelling of these dispersion processes has to rely in models that take into account the canopy geometry explicitly, as CFD-based fast-response models (e.g. Patnaik and Boris, 2007; Carruthers et al., 2012) and street network models (Soulhac et al., 2011).

6.2. Vertical exchange velocity

Street network models (Hamlyn et al. 2007; Soulhac et al, 2011) adopt 'ad hoc' simplified relations to quantify the mass fluxes within and above the urban canopy. A key parameter for this modelling approach is the 'exchange velocity', referred to here as u_e, which represents an estimate of the vertical pollutant fluxes between the street canyons and the overlying atmosphere. Existing models for u_e (Bentham and Britter, 2003; Soulhac et al., 2013) do not include explicitly any dependence on the street canyon geometry and wind incident angle θ. However, recent studies (Ben Salem et al., 2015) have shown that the performance of these models can be improved by finer parameterizations of u_e, namely by adopting empirical corrections (Soulhac et al., 2013) as a function of the wind incident angle θ. This finding motivates the need for direct estimates of u_e based on both numerical simulations and wind tunnel experiments.

Strictly speaking, u_e can be regarded as a bulk velocity scale (e.g. Bentham and Britter, 2003; Solazzo and Britter, 2007; Solazzo et al., 2010), or an exchange ratio, that can be used as a surrogate for the complex transfer processes between the canopy and the overlying atmosphere (Salizzoni et al., 2010; Perret and Savory, 2013). This is defined as:

$$u_e = \frac{q_v}{A_{roof}\left(\left\langle \overline{C}_{canopy} \right\rangle - \left\langle \overline{C}_{bkg} \right\rangle\right)} \tag{7}$$

where $\left\langle \overline{C}_{canopy} \right\rangle$ denotes the spatially-averaged pollutant concentration within the urban canopy and $\left\langle \overline{C}_{bkg} \right\rangle$ is the background concentration, i.e. the pollutant concentration of the incoming atmospheric flow (which here is set equal to zero) and where $q_V = \iint_{A_{roof}} \left(\overline{c}.\overline{w} + \overline{c'w'}\right) dA$ is the pollutant flux at roof level through the exchange surface A_{roof}. The latter is given by the sum of a mean $q_m = \iint_{A_{roof}} \overline{c}.\overline{w} dA$ and a turbulent $q_T = \iint_{A_{roof}} \overline{c'w'} dA$ contribution ($\overline{c'w'}$ indicates the correlation between fluctuations of vertical velocity and concentration).

In this study we are interested in showing the dependence of u_e on slight modifications of the urban geometry and of the wind incident angle. It is questionable if RANS closure models can provide reliable estimates of u_e, given the high intermittency characterising the exchange between the canyon and the overlying flow. This topic was the subject of a detailed study by Moonen et al. (2011) concerning the ventilation of a square section canyon of varying length, by means of RANS and LES simulations. Their results show that RANS simulations generally tend to smooth the dependence of u_e on the wind direction for small canyons, i.e. length of the canyon less than $2H$, and may induce errors of more than 100%, depending on the wind direction. However, the difference between the two numerical models is progressively reduced for increasing canyon lengths, and is of order 20% for a length of the canyon ≥10H. Results also show that, as the length of the canyon attains and exceeds 5H, RANS simulations are able to capture the general tendencies of the dependence u_e on the wind direction, although generally underestimating LES predictions of u_e. For these reasons, we are confident that our simulations provide reliable information on the dependence of u_e on wind direction and street aspect ratios. Assuming the results of Moonen et al. (2011) as a reference, even though the form of the canyons considered here is somehow different to that they simulated, we expect our estimates of the exchange velocity to be affected by differences of about 20% with respect to similar estimates provided by LES simulations.

Values of u_e have been here inferred from those of the total flux of mass q_V, that have been computed as the residual of a balance of the pollutant fluxes entering and leaving the array through the sections of the streets at its borders. In stationary conditions, the integral mass balance over the whole array can be written as:

$$\int_V Q_U dV = q_V + \int_A \left(\bar{U}_i \cdot \bar{C} + \overline{u_i'c'}\right) \cdot n_i dA \tag{8}$$

where $\bar{C}$ is the averaged concentration, Q_U is the passive scalar emission rate per unit volume within the array, A is the total surface of the street sections at the border of the neighbourhood, V is the volume of air contained in it and $\overline{u_i'c'}$ are the three component of the turbulent scalar fluxes. The last two flux terms on the r.h.s. of Eq. (8) denote the mean and turbulent mass transfer trough the vertical section of the street at the canopy lateral border. These latter fluxes were computed from the numerical results as:

$$\overline{u_i'c'} = -D_t \frac{\partial \bar{C}}{\partial x_i} \tag{9}$$

where $D_t = \dfrac{\nu_t}{Sc_t}$ is the turbulent diffusivity of mass, estimated as the ratio of the turbulent viscosity ν_t and the turbulent Schmidt number Sc_t.

The vertical exchange velocity u_e was then estimated for each configuration by means of Eq. (7). To that end the concentration within the array $\langle C_{canopy} \rangle$ was computed as a volume integral from the CFD results. Table 4 summarizes the values of u_e obtained by CFD simulations and normalized by $u_* = 0.23\text{ms}^{-1}$ (Garbero et. al., 2010).

Table 4 about here

Our estimates of the non-dimensional exchange velocity show limited discrepancies (± 20% approximately) with the predictions of the model formulated by Soulhac et al. (2013), i.e. $u_e/u_* \approx 0.27$, and Bentham and Britter (2003), i.e. $u_e/u_* \approx 0.3$. Exchange velocities are also always larger than those measured by Salizzoni et al. (2009) ($u_e/u_* \approx 0.2$) in two dimensional street canyons. This difference can be easily explained by the fact that part of the mass exchange mechanisms observed in 3D geometries do not take place in a two-dimensional canyon, namely those associated to the vertical mean and turbulent fluxes at street intersections and close to the street lateral borders.

Comparing our results with estimates from previous numerical studies requires to normalise u_e with a reference velocity U_{ref}, taken at 2.5H (see Hamlyn and Britter, 2005). In our case u_e is about 2-5% of U_{ref}, depending on the configuration, a range that compares favourably well to those reported by Solazzo and Britter (2007), Hamlyn and Britter (2005) and Panagiotou et al. (2013). Solazzo and Britter (2007) showed that, in an isolated canyon with an external wind blowing perpendicularly to the street axis, u_e is approximately around 1% of U_{ref}. Hamlyn and Britter (2005) and Panagiotou et al. (2013) show that the variations of u_e can by hardly correlated to those of λ_p and generally lay in the range 2% - 10% U_{ref}. As a further remark, we point out that the values of u_e/u_* in Table 4 appear to be almost decoupled from those of the vertical flow rates (Fig. 9). This confirms that the value of the flow rate can induce misleading information concerning the effectiveness of canopy ventilation and cannot be used as a reliable parameter for estimates of city breathability in compact arrays.

For each angle, u_e/u_* values for Configuration 1 are lower than those obtained in the two other configurations, which have larger total exchange area at roof top, and therefore lower λ_p (λ_p=0.69 for Configuration 1 and λ_p=0.59 Configuration 2 and 3). Significant variations of u_e/u_* can be however observed also for a fixed array geometry, as the wind incident angle varies. For Configuration 1 the ratio ${u_e}/{u_*}$ for θ=*47.5°* is almost 50% larger than that for θ=*2.5°*. The significant dependence on the angle θ is also demonstrated by the different values obtained for Configurations 2 and 3 for θ=47.5°, which in fact are the same geometrical configurations, rotated of 5° (i.e. Configuration 3 is the same as Configuration 2 rotated by an angle of 90°, thus Configuration 3 subjected to a wind direction θ=47.5° corresponds to Configuration 2 subjected to a wind direction θ=42.5°, see Section 2 and Fig. 2).

An increased exchange area is therefore only partially responsible for an enhancement of the vertical exchange. This has therefore to be attributed to a general variation of the flow dynamics within the array. In particular, our results (Fig. 11) suggest that an increase of ${u_e}/{u_*}$ can be due to an enhancement of the mean counterpart q_m of the total vertical flux q_V. Values of the ratio $\frac{q_m}{q_V}$ for corresponding ${u_e}/{u_*}$ are given in Table 5, which shows that $\frac{q_m}{q_V}$ increases for increasing θ (this happens for all configuration except for Configuration 3, as θ=12.5°). This trend confirms the qualitative analysis presented in Subsection 5.1 concerning the mean flow patterns within the array, as visualized by the mean streamlines. A larger θ is generally responsible for a higher complexity of the streamline topology, resulting in a higher interaction between the mean flow developing above the canopy and within it. Minimal values of $\frac{q_m}{q_V}$ are observed for Configuration 2 and θ=*2.5°*, as a consequence of the strong channelling along large roads (Panagiotou et al., 2013) whose axis is almost perpendicular to the wind direction (Soulhac and Salizzoni, 2010). The largest value of $\frac{q_m}{q_V}$ for each configuration are obtained for θ=*47.5°* as the mean flow streamlines produce the most complex patterns (Fig. 8).

Table 5 about here

Fig. 11 about here

The linear fitting of the data in Table 5 and Fig. 11 provides a relation of the form:

$$\frac{u_e}{u_*} = a\frac{q_m}{q_V} + b \tag{10}$$

where the values of the constant a and b varies depending on the data used to fit the regression line. When all data are fitted we obtain $a = 0.27$ and $b = 0.22$, values that are also obtained when fitting the data for Configuration 2 and 3. Conversely, when data for Configuration 1 are only considered, the value of a is slightly larger and that of b is slightly lower.

Although purely empirically derived, the trend of Eq. (10) and its form can be interpreted physically. The term $a\frac{q_m}{q_V}$ indicates that the increase of u_e/u_* is related to an increased contribution of the mean fluxes, that generally increase with θ. This is clearly linked with the topology of the mean streamlines (see Fig. 8) which becomes more complex for larger wind angles. The constant b represents the turbulent counterpart of the exchange which holds when the mean vertical flow is suppressed, as it happens in 2D street canyons. It is worth noting that the value of b is in close agreement with the direct estimate $u_e/u_* \approx 0.2$ achieved experimentally by Salizzoni et al. (2009).

It is to note that existing parameterisations of u_e/u_* are based only on the estimates of the turbulent counterpart of the exchange and neglect any possible influence of the street aspect ratio and wind incidence angle. Therefore, the parameterisations currently adopted in urban dispersion models have to be handled with caution, since the canopy/atmosphere transfer is shown to be significantly sensitive to both wind direction and street aspect ratios. In order to improve these bulk exchange models, a parameterisation of the contribution of the mean flow would then be necessary to include the effects of a varying θ on u_e/u_*.

7. Conclusions

In this paper we analysed pollutant dispersion and ventilation conditions within densely packed group of obstacles representative of central European neighbourhoods in terms of packing density (expressed though the morphometric parameters λ_p and λ_f), though in simplified form. This kind of urban configurations, even though usually associated to high traffic levels and densities of population, have been rarely studied in the literature. Exploring ventilation conditions in this type of urban neighbourhood is indeed crucial for the assessment of air quality scenarios and their impacts on human health for a consistent part of the population of European countries.

To this aim, we performed CFD RANS simulations focusing on the influence of a varying wind direction and of slight modification of the geometrical parameters of the building array. Simulations were performed to estimate parameters that would be difficult to measure experimentally, i.e. the mean flow rate, the mean age of air and the exchange velocity which, all together, provided a measure of “city breathability” of compact arrays. Robustness of numerical simulations was preliminarily tested through detailed comparisons with measurements of flow velocity and passive scalar concentration from previous wind tunnel experiments.

Results showed that, differently from what observed in sparse arrays, the mean flow rate did not exhibit a clear dependence of the geometry and wind direction and therefore it is not suitable for assessing ventilation conditions in compact cities. Conversely, the mean age of air revealed a high variability of ventilation conditions depending on the incident wind angle and slight modifications of the array’s geometry. These varying ventilation conditions have been explained by a detailed analysis of the mean flow streamlines and the exchange velocity.

Specifically, for low wind angles we observed a clear effect of channelling of pollutants along the street parallel to the wind direction. This effect, combined with relative low exchanges at street intersections and with the overlying atmosphere, results in poor ventilation conditions. Conversely, large wind angles are shown to enhance transversal mean transfers at street intersections and vertical exchange with overlying atmosphere. The analysis of the exchange velocity further clarified that, for increasing incident angles, the vertical transfer increases due to the enhancement of the mean counterpart of the total flux. As evidenced from the mean flow streamlines topology, whose 3-D structure becomes more complex as the wind incident angle increases, this effect was associated to a stronger interaction between the mean flow developing above the canopy and that within it.

The strong variability of the ventilation conditions due to changing wind directions and slight variations in the array geometry, which in turn induce little variations in the morphometric parameters λ_p and λ_f, implies evident shortcomings for the adoption of urban models that describe the spatially-averaged ventilation conditions based on a reduced set of morphometric parameters.

Our analysis also suggests the need of (i) taking into account the mean advective vertical mass fluxes, whose intensity was shown to be sensitive to the wind direction, and (ii) considering the parameterisation of a bulk vertical exchange velocity characterising the transfer between the canopy and the overlying atmosphere.

Overall, the results presented here clearly show that the identification of a reduced set of parameters assessing the flow and pollutant dispersion within a city neighbourhood, without computationally expensive CFD simulations, still remains a challenge for a comprehensive evaluation of the breathability of compact cities.

Acknowledgements

This study was supported by the ANR (AIR-Q project 2012-14), by the Region Rhône Alpes and by Regione Piemonte via the project "AirToLiMi: Modelling and simulating sustainable mobility strategies. A study of three real test cases: Turin, Lyon, Milan" (CIPE 2006).

References

Barth, T.J., Jespersen, D., 1989. The design and application of upwind schemes on unstructured meshes. Technical Report AIAA-89-0366. In: AIAA 27th Aerospace Sciences Meeting, Reno, Nevada.

Bentham, J.T., Britter, R.E., 2003. Spatially averaged flow within obstacle arrays. Atmospheric Environment 37, 2037-2043.

Ben Salem, N., Garbero, V., Salizzoni, P., Lamaison, G., Soulhac, L., 2015. Modelling pollutant dispersion in a street network. Boundary-Layer Meteorology 155, 157-187.

Buccolieri, R., Sandberg, M., Di Sabatino, S., 2010. City breathability and its link to pollutant concentration distribution within urban-like geometries. Atmospheric Environment 44, 1894-1903.

Carruthers, D., Di Sabatino, S. and Hunt, J., 2012. Urban air quality: meteorological processes. In Meyers, R. (Ed.): Encyclopedia of Sustainability Science and Technology, Article No. 00427, Publisher Springer.

Carpentieri, M., Salizzoni, P., Robins, A. and Soulhac, L., 2012. Evaluation of a neighbourhood scale, street network dispersion model through comparison with wind tunnel data. Environmental Modelling & Software 37, 10–124.

Coceal, O., Belcher, S.E., 2004. A canopy model of mean winds through urban areas. Quarterly Journal of the Royal Meteorological Society 130, 1349–1372.

Coceal, O., Dobre, A., Thomas, T.G., 2007. Unsteady dynamics and organized structures from DNS over an idealized building canopy. International Journal of Climatology 27, 1943-1953.

Dallman, A., Di Sabatino, S., Fernando, H.J.S., 2013. Flow and turbulence in an industrial/suburban roughness canopy. Environmental Fluid Mechanics 13, 279-307.

Dejoan, A., Santiago, J.L., Martilli, A., Martin, F., Pinelli, A., 2010. Comparison between Large-Eddy and Reynolds-Averaged Navier-Stokes computations for the MUST field experiment. Part II: Effects of incident wind angle deviation on the mean flow and plume dispersion. Boundary-Layer Meteorology 135, 133-150.

Di Sabatino, S., Leo, L.S., Cataldo, R., Ratti, C., Britter, R.E., 2010. Construction of digital elevation models for a southern European city and a comparative morphological analysis with respect to Northern European and North American cities. Journal of Applied Meteorology and Climatology 49, 1377-1396.

Di Sabatino, S., Buccolieri, R., Olesen, H.R., Ketzel, M., Berkowicz, R., Franke, J., Schatzmann, M., Schlunzen, K.H., Leitl, B., Britter, R., Borrego, C., Costa, A.M., Trini Castelli, S., Reisin, T.G., Hellsten, A., Saloranta, J., Moussiopoulos, N., Barmpas, F., Brzozowski, K., Goricsan, I., Balczo, M., Bartzis, J.G., Efthimiou, G., Santiago, J.L., Martilli, A., Piringer, M., Baumann-Stanzer, K., Hirtl, M., Baklanov, A.A., Nuterman, R.B., Starchenko, A.V., 2011a. COST 732 in practice: the MUST model evaluation exercise. Int. J. Environment and Pollution 44, 403-418.

Di Sabatino, S., Buccolieri, R., Paradisi, P., Palatella, L., Corrado, R., 2011b. A fast model for pollutant dispersion at the neighbourhood scale. International Journal of Environment and Pollution 47, 207–215.

Di Sabatino, S., Buccolieri, R., Salizzoni, P., 2013. Recent advancements in numerical modelling of flow and dispersion in urban areas: a short review. International Journal of Environment and Pollution 52, 172-191.

Etheridge, D., Sandberg, M., 1996. Building Ventilation: Theory and Measurement. John Wiley & Sons, Chichester.

Fernando, H.J.S., Zajic, D., Di Sabatino, S., Dimitrova, R., Hedquist, B., Dallman, A., 2010. Flow, turbulence, and pollutant dispersion in urban atmospheres. Physics of Fluids 22, 1-20.

Fluent, 2006. User’s Manual. http://www.fluent.com

Garbero, V., Salizzoni, P., Soulhac, L., 2010. Experimental study of pollutant dispersion within a network of streets. Boundary-Layer Meteorology 136, 457-487.

Gousseau, P., Blocken, B. and van Heijst, G.J.F., 2011. CFD simulation of pollutant dispersion around isolated buildings: on the role of convective and turbulent mass fluxes in the prediction accuracy. Journal of Hazardous Materials 194, 422–434.

Hamlyn, D., Britter, R.E., 2005. A numerical study of the flow field and exchange processes within a canopy of urban-type roughness. Atmospheric Environment 39, 3243-3254.

Hamlyn, D., Hilderman, T., Britter, R., 2007. A simple network approach to modelling dispersion among large groups of obstacles. Atmospheric Environment 41, 5848–5862.

Hang, J., Sandberg, M., Li, Y.G., 2009. Age of air and air exchange efficiency in idealized city models. Building and Environment 44, 1714-1723.

Hang, J., Li, Y., Sandberg, M., Buccolieri, R., Di Sabatino, S., 2012a. The influence of building height variability on pollutant dispersion and pedestrian ventilation in idealized high-rise urban areas. Building and Environment 56, 346–360.

Hang, J., Li, Y., Buccolieri, R., Sandberg, M., Di Sabatino, S., 2012b. On the contribution of mean flow and turbulence to city breathability: the case of long streets with tall buildings. Science of the Total Environment 416, 362-373.

Hoydysh, W.G., Dabberdt, W.F., 1994. Concentration fields at urban intersections: fluid modeling studies. Atmospheric Environment 28, 1849–1860.

Huq, P., Franzese, P. 2013. Measurements of turbulence and dispersion in three idealized urban canopies with different aspect ratios and comparisons with a Gaussian Plume Model. Boundary-Layer Meteorology 147, 103-121.

Launder, B.E., Spalding, D.B., 1974. The numerical computation of turbulent flows. Computer Methods in Applied Mechanics and Engineering 3, 269-289.

Moonen, P., Dorer, V., Carmeliet, J., 2011. Evaluation of the ventilation potential of courtyards and urban street canyons using RANS and LES. Journal of Wind Engineering and Industrial Aerodynamics 99, 414-423.

Murena, F., Di Benedetto, A., D'Onofrio, M., Vitiello, G., 2011. Mass transfer velocity and momentum vertical exchange in simulated deep street canyons. Boundary-Layer Meteorology 140, 125-142.

Neophytou M.K.-A., Markides, C.N., Fokaides, P.A., 2014. An experimental study of the flow through and over two dimensional rectangular roughness elements: Deductions for urban boundary layer parameterizations and exchange processes. Physics of Fluids 26, 086603.

Oke, T.R., 1988. Street design and urban canopy layer climate. Energy Building 11, 103-113.

Panagiotou, I., Neophytou, M.K.-A., Hamlyn, D., Britter, R.E., 2013. City breathability as quantified by the exchange velocity and its spatial variation in real inhomogeneous urban geometries: An example from central London urban area. Science of The Total Environment 442, 466-477.

Patnaik, G., Boris, J.P., 2007. Fast and accurate CBR defense for homeland security: bringing HPC to the first responder and warfighter. Proc. HPCMP Users Group Conference 2007; High Performance Computing Modernization Program: A Bridge to Future Defense, DoDHPCMP UGC, Art. No. 4437973, 120–126.

Perret, L., Savory, E., 2013. Large-scale structures over a single street canyon immersed in an urban-type boundary layer. Boundary-Layer Meteorology 148, 111–131.

Ratti, C., Di Sabatino, S., Britter, R., 2006. Urban texture analysis with image processing techniques: wind and dispersion. Theoretical and Applied Climatology 84, 77-99.

Salizzoni, P., Soulhac, L., Mejean, P., 2009. Street canyon ventilation and atmospheric turbulence. Atmospheric Environment 43, 5056-5067.

Salizzoni, P., Van Liefferinge, R., Mejean, P., Soulhac, L., Perkins, R.J., 2010. Scaling of the vertical spreading of a plume of a passive tracer in a rough-wall neutral boundary layer. Boundary-Layer Meteorology 135, 455-467.

Salim, S.M., Buccolieri, R., Chan, A., Di Sabatino, S., 2011. Numerical simulation of atmospheric pollutant dispersion in an urban street canyon: Comparison between RANS and LES. Journal of Wind Engineering & Industrial Aerodynamics 99, 103-113.

Santiago, J.L., Coceal, O., Martilli, A., Belcher, S.E., 2008. Variation of the sectional drag coefficient of a group of buildings with packing density. Boundary-Layer Meteorology 128, 445-457.

Santiago, J.L. Martilli, A., 2010. A dynamic urban canopy parameterization for mesoscale models based on computational fluid dynamics Reynolds-averaged Navier-Stokes microscale simulations. Boundary-Layer Meteorology 137, 417-439.

Santiago, J.L., Krayenhoff, E.S., Martilli, A., 2014. Flow simulations for simplified urban configurations with microscale distributions of surface thermal forcing. Urban Climate 9, 115-133.

Solazzo, E., Britter, R.E., 2007. Transfer processes in a simulated urban street canyon. Boundary-Layer Meteorology 124, 43-60.

Solazzo, E., Di Sabatino, S., Aquilina, N., Dudek, A., Britter, R., 2010. Coupling mesoscale modelling with a simple urban model: the Lisbon case study. Boundary-Layer Meteorology 137, 441-457.

Soulhac, L., Garbero, V., Salizzoni, P., Mejean, P., Perkins, R.J., 2009. Flow and dispersion in street intersections. Atmospheric Environment 43, 2981-2996.

Soulhac, L., Salizzoni, P., 2010. Dispersion in a street canyon for a wind direction parallel to the street axis. Journal of Wind Engineering and Industrial Aerodynamics 98, 903-910.

Soulhac, L., Salizzoni, P., Cierco, F.X., Perkins, R.J., 2011. The model Sirane for atmospheric urban pollutant dispersion; PART I, presentation of the model. Atmospheric Environment 45, 7379-7395.

Soulhac, L, Salizzoni, P., Mejean, P., Perkins, R.J., 2013. Parametric laws to model urban pollutant dispersion with a street network approach. Atmospheric Environment 67, 229–241.

Tominaga, Y., Stathopoulos, T., 2013. CFD simulation of near-field pollutant dispersion in the urban environment: A review of current modeling techniques. Atmospheric Environment 79, 716-730.

Venkatram, A., Isakov, V., Yuan, J., Pankratz, D., 2004. Modeling dispersion at distances of meters from urban sources. Atmospheric Environment 38, 4633-4641.

Yee, E., Biltoft, C.A., 2004. Concentration fluctuation measurements in a plume dispersing through a regular array of obstacles. Boundary-Layer Meteorology 111, 363-415.

Yim, S.H.L., Fung, J.C.H., Lau, A.K.H., Kot, S.C., 2009. Air ventilation impacts of the “wall effect” resulting from the alignment of high-rise buildings. Atmospheric Environment 43, 4982–4994.

Zajic, D., Fernando, H.J.S., Brown, M.J., Pardyjak, E.R., 2015. On flows in simulated urban canopies. Environmental Fluid Mechanics 15, 275-303.

Figure captions

Fig. 1. View of typical European city neighbourhoods: (a) Barcelona, Spain, (b) Lyon, France, (c) Bari, Italy and (d) Turin, Italy.

Fig. 2. Diagram showing configurations (model scale 1:400), source position (black point) and wind directions θ.

Fig. 3. Vertical profiles of non-dimensional mean longitudinal velocity (a), turbulent kinetic energy (k) (b) and k dissipation ε (c). Symbols refer to wind tunnel measurements of Garbero et al. (2010) above the obstacle array. Dot-dashed lines refer to the inlet profiles imposed in the CFD numerical simulations, correpsonding to (a) Eq. (1), (b) Eq. (2) and (c) Eq. (3).

Fig. 4. (a) 3D schematic sketch of geometry and boundary conditions used in CFD simulations and (b) building array showing the reference upstream area A_{ref} (grey) used for the calculation of the normalized flow rates.

Fig. 5. Normalized mean velocity horizontal (u/U_H and v/U_H, top and middle) and vertical (w/U_H, bottom) profiles along the dashed lines at street intersection for (a) Configuration 1 and (b) Configuration 2 at x=0 (point source position, see Fig. 2) and z=H/2 for wind direction θ=2.5°.

Fig. 6. Normalized mean velocity horizontal (u/U_H and v/U_H, left) and vertical (w/U_H, right) profiles along the dashed line (first street on the right with respect to the source position) at street intersection for Configuration 1 (S_x=S_y=H) and z=H/2 for wind direction θ=47.5°.

Fig. 7. Normalized concentrations c^+ along the dashed lines (third street on the right with respect to the source) at z=H/2 for wind directions θ=2.5° and 47.5° for (a,c) Configuration 1, (b) Configuration 2 and (d) Configuration 3.

Fig. 8. Mean flow streamlines for (a,c) Configuration 1 and (b,d) Configuration 3 with θ=2.5° and 47.5°. The wind blows from the left inclined by (a,b) 2.5° and (c,d) 47.5° to the x-direction (see **Fig. 2**).

Fig. 9. Normalized flow rates for approaching wind direction (a) θ=2.5°, (b) θ=12.5°, (c) θ=27.5° and (d) θ=47.5°. The flow rate is positive for air entering the array and negative for air leaving the array.

Fig. 10. Normalized mean age of air at pedestrian level for wind direction (a) θ=2.5°, (b) θ=12.5°, (c) θ=27.5° and (d) θ=47.5°.

Fig. 11. Non-dimensional exchange velocity ${}^{u_e}\!/\!{}_{u_*}$ as a function of the ratio q_m / q_V (the mean mass flux to the total vertical flux) and linear fitting (dashed line) for the three configuration studied.

fig.1_final.tif

fig.1_bw_final.tif

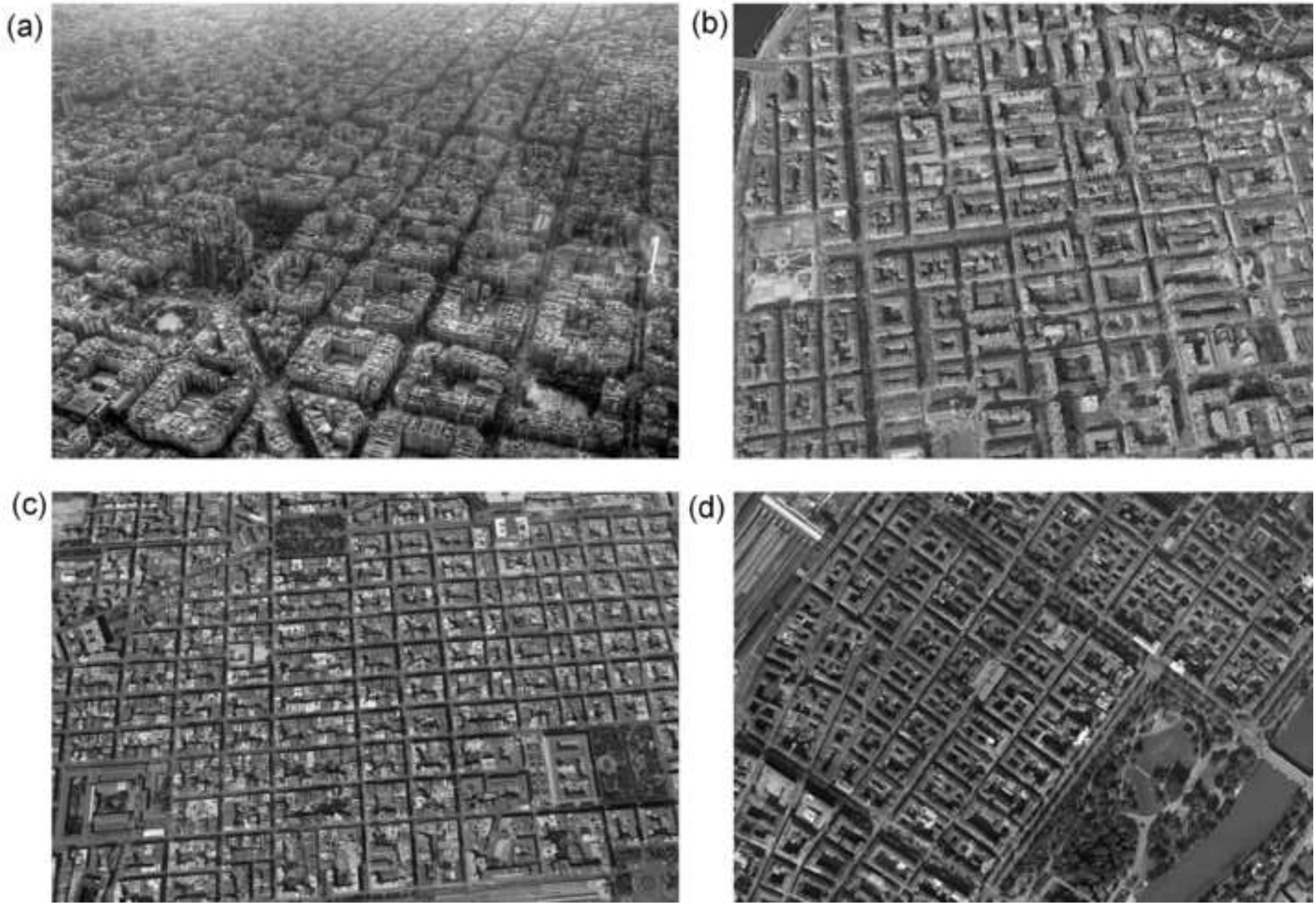

fig.2_final.tif

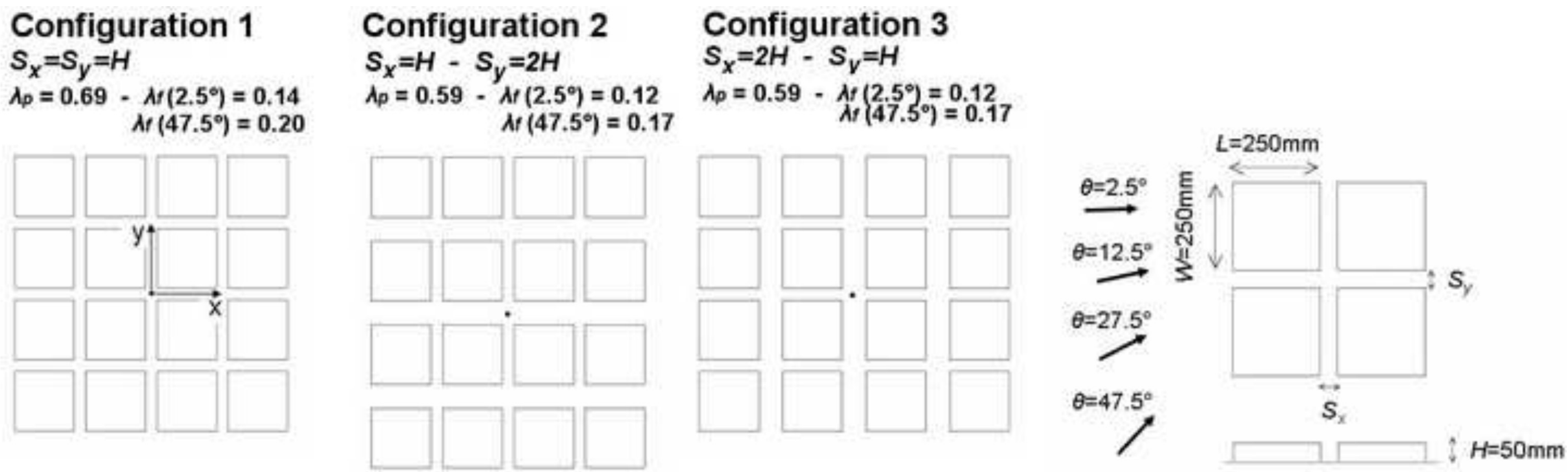

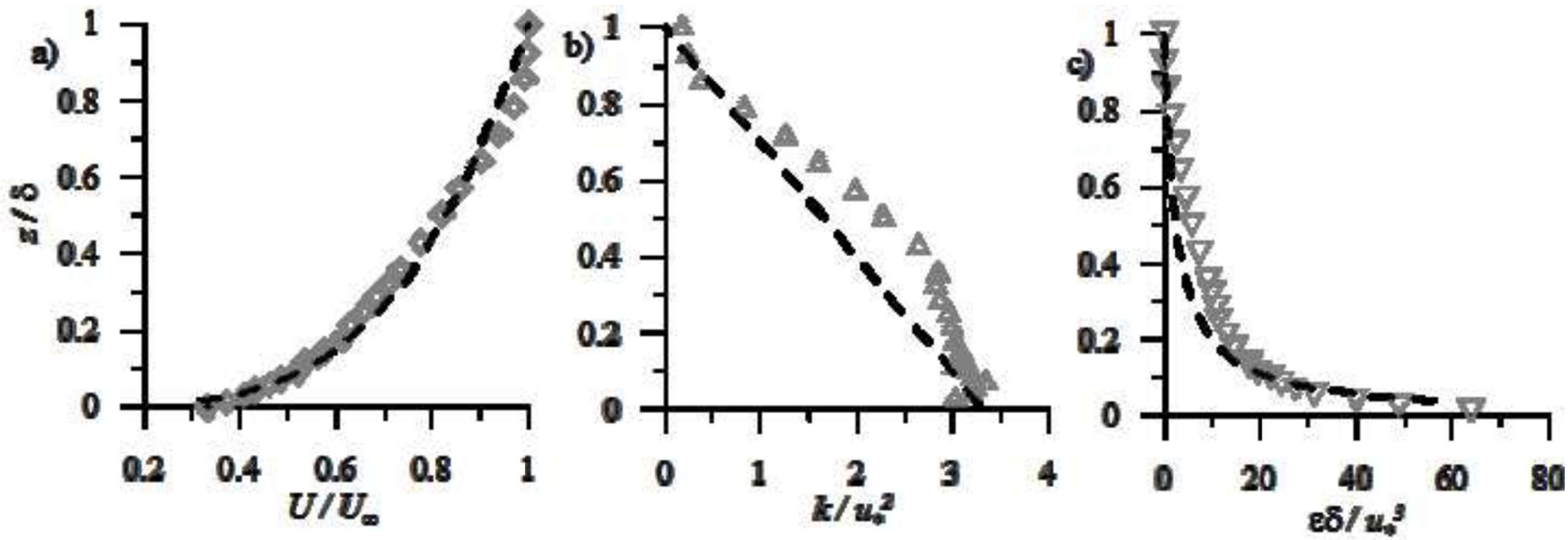
a)
b)
c)
z/δ
U/U_∞
k/u_*^2
$\varepsilon\delta/u_*^3$

fig.4_final.tif
Click here to download high resolution image

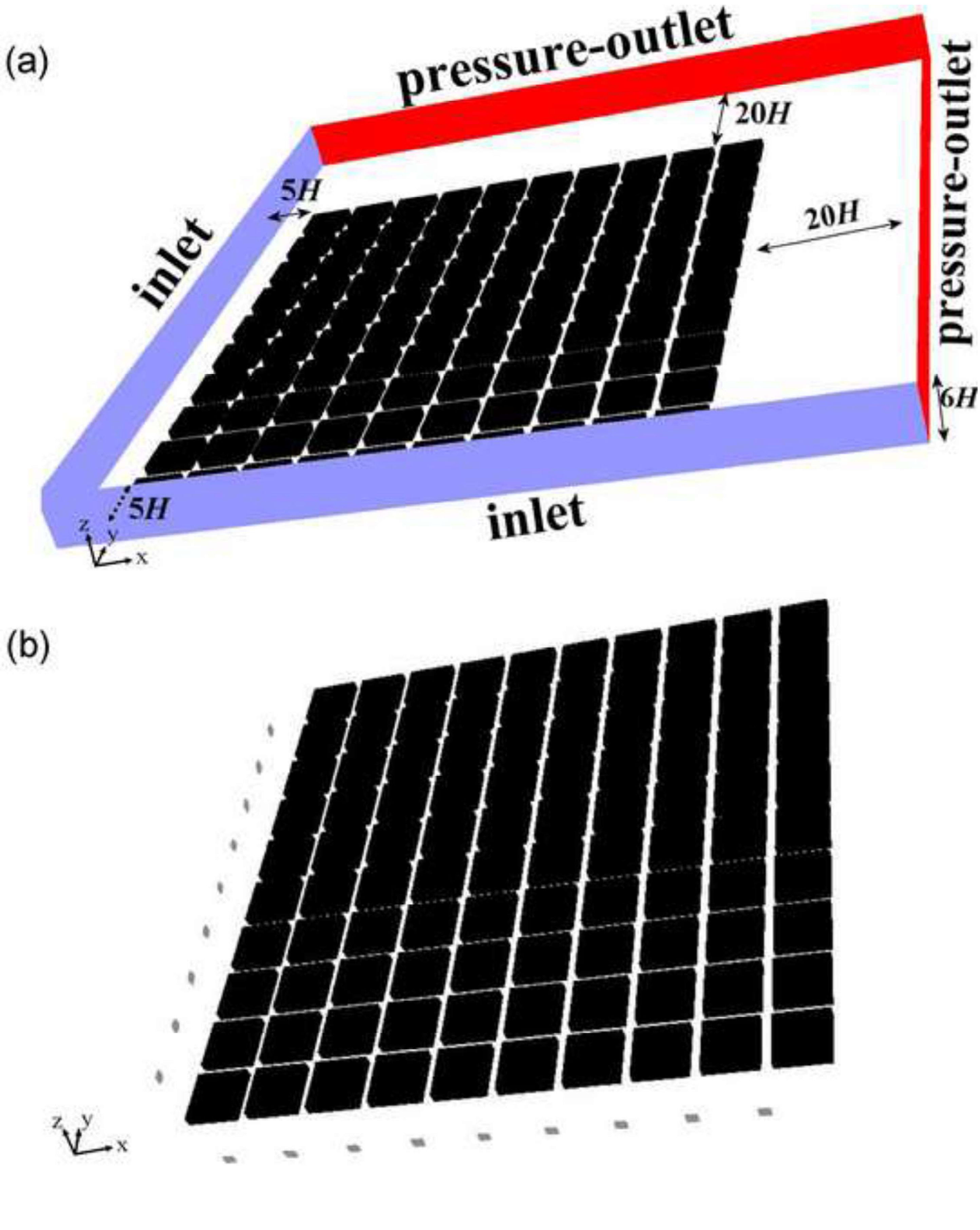

fig.4_bw_final.tif
Click here to download high resolution image

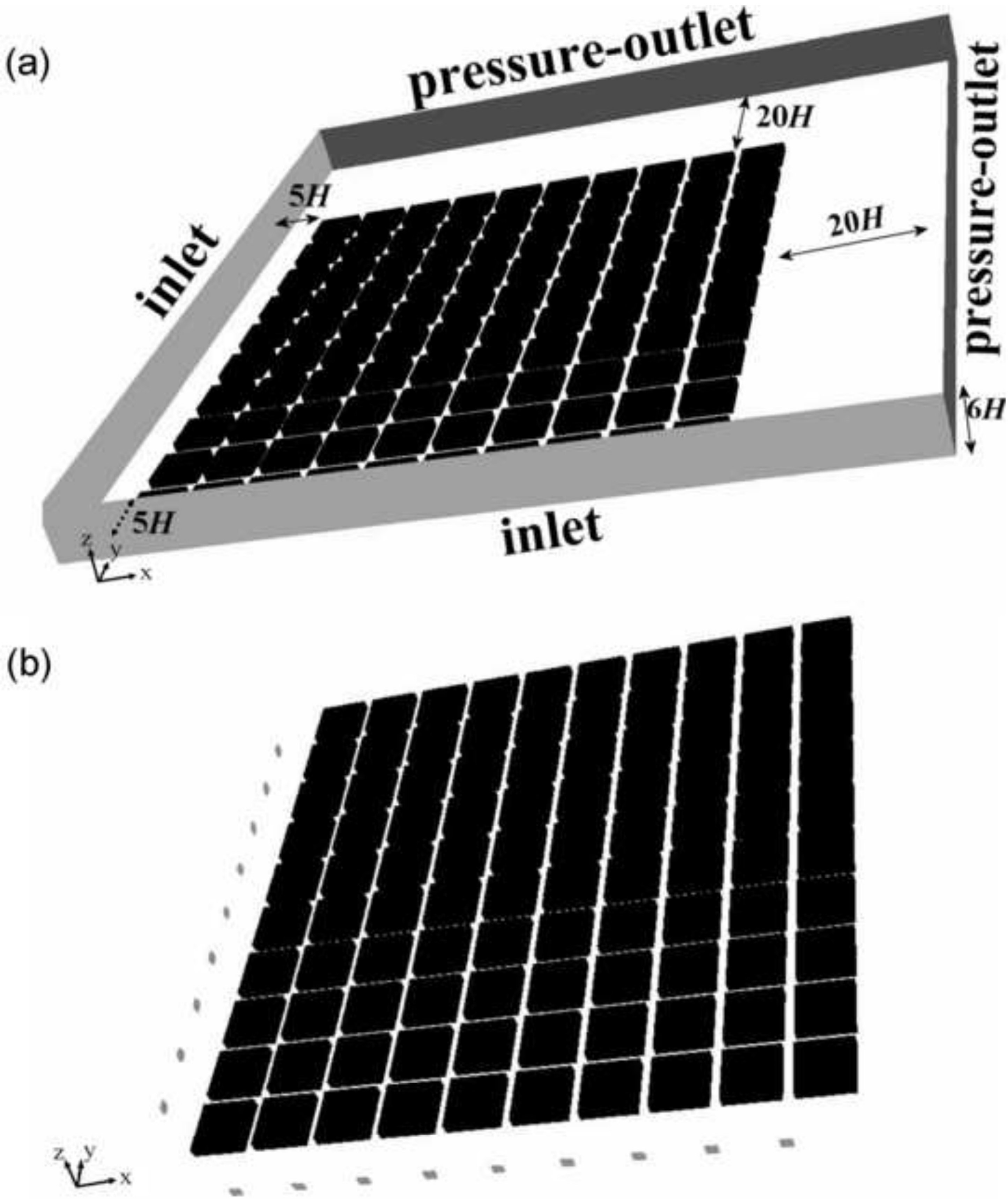

fig.5_final.tif
Click here to download high resolution image

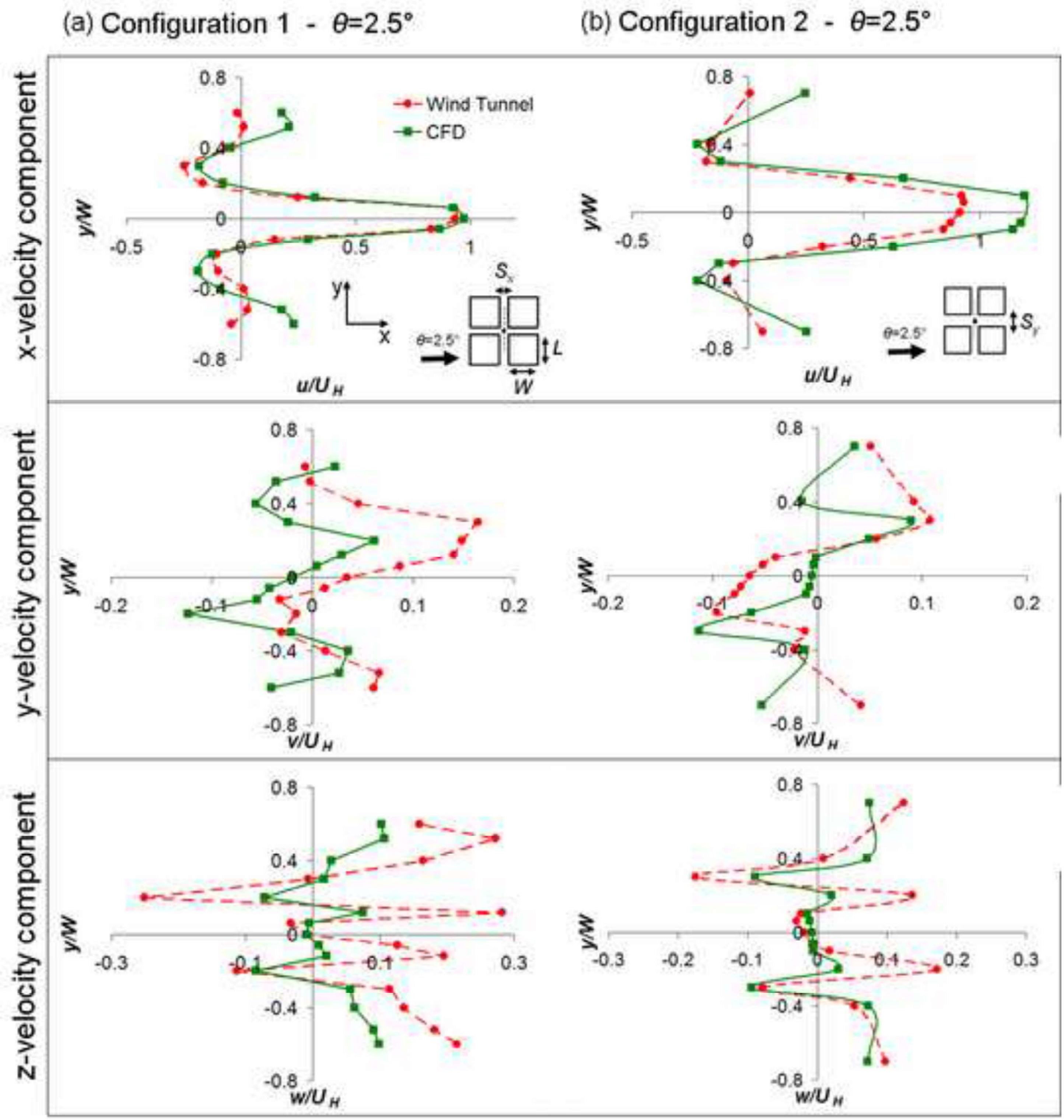

fig.5_bw_final.tif
Click here to download high resolution image

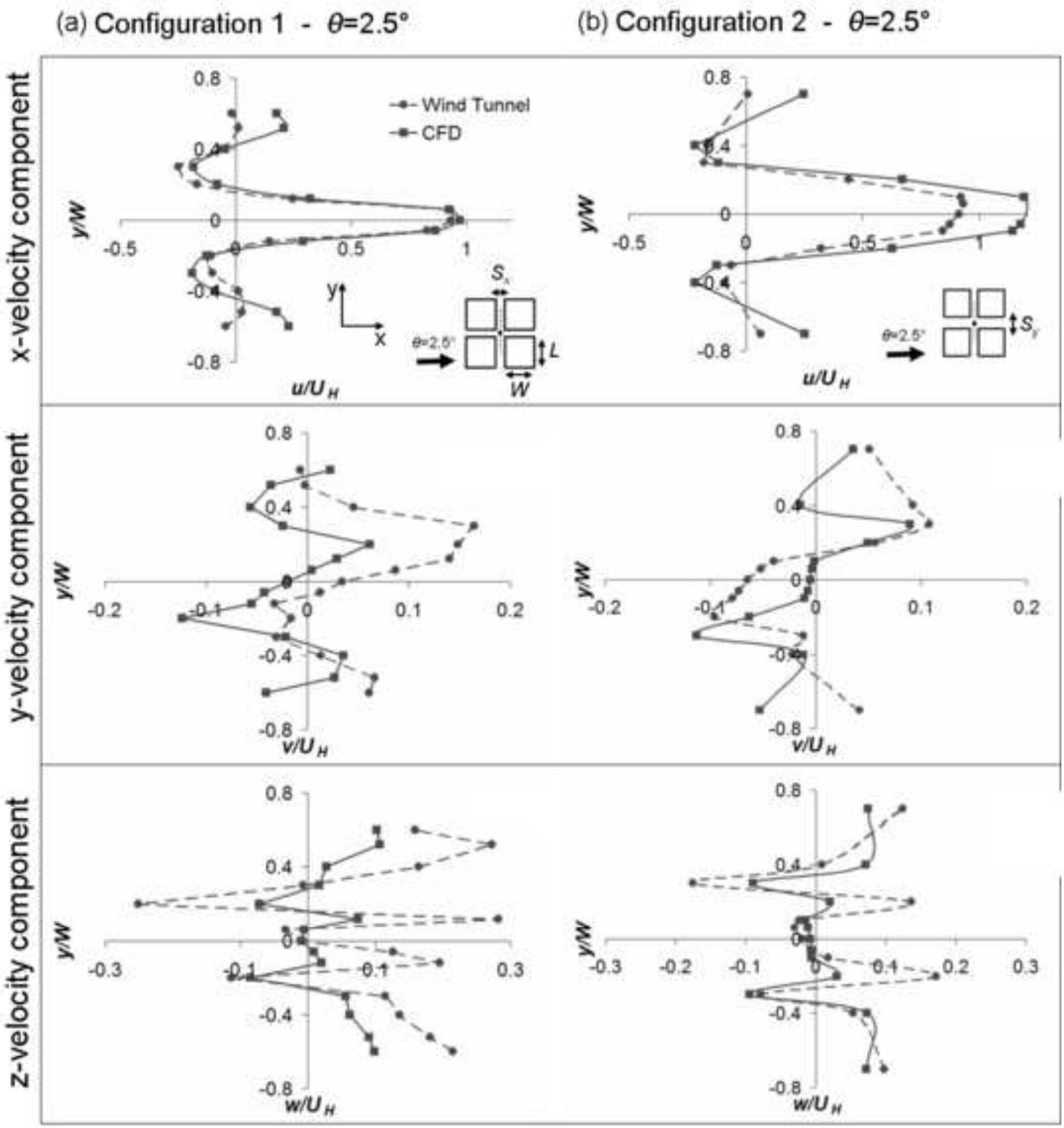

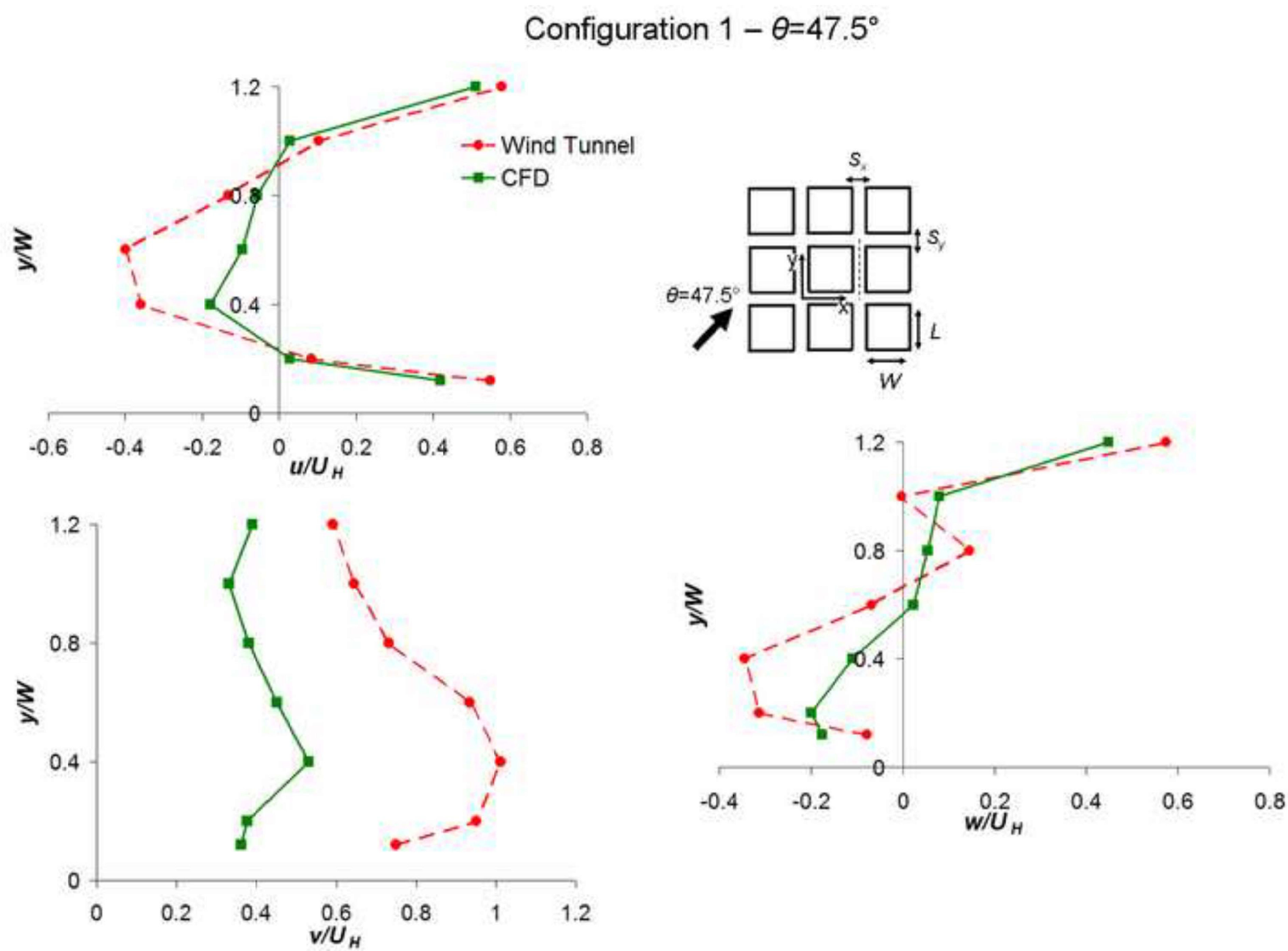
Configuration 1 – θ=47.5°
Wind Tunnel
CFD
y/W
u/U_H
v/U_H
w/U_H
θ=47.5°
S_x
S_y
L
W
x
y
-0.6
-0.4
-0.2
0
0.2
0.4
0.6
0.8
1
1.2

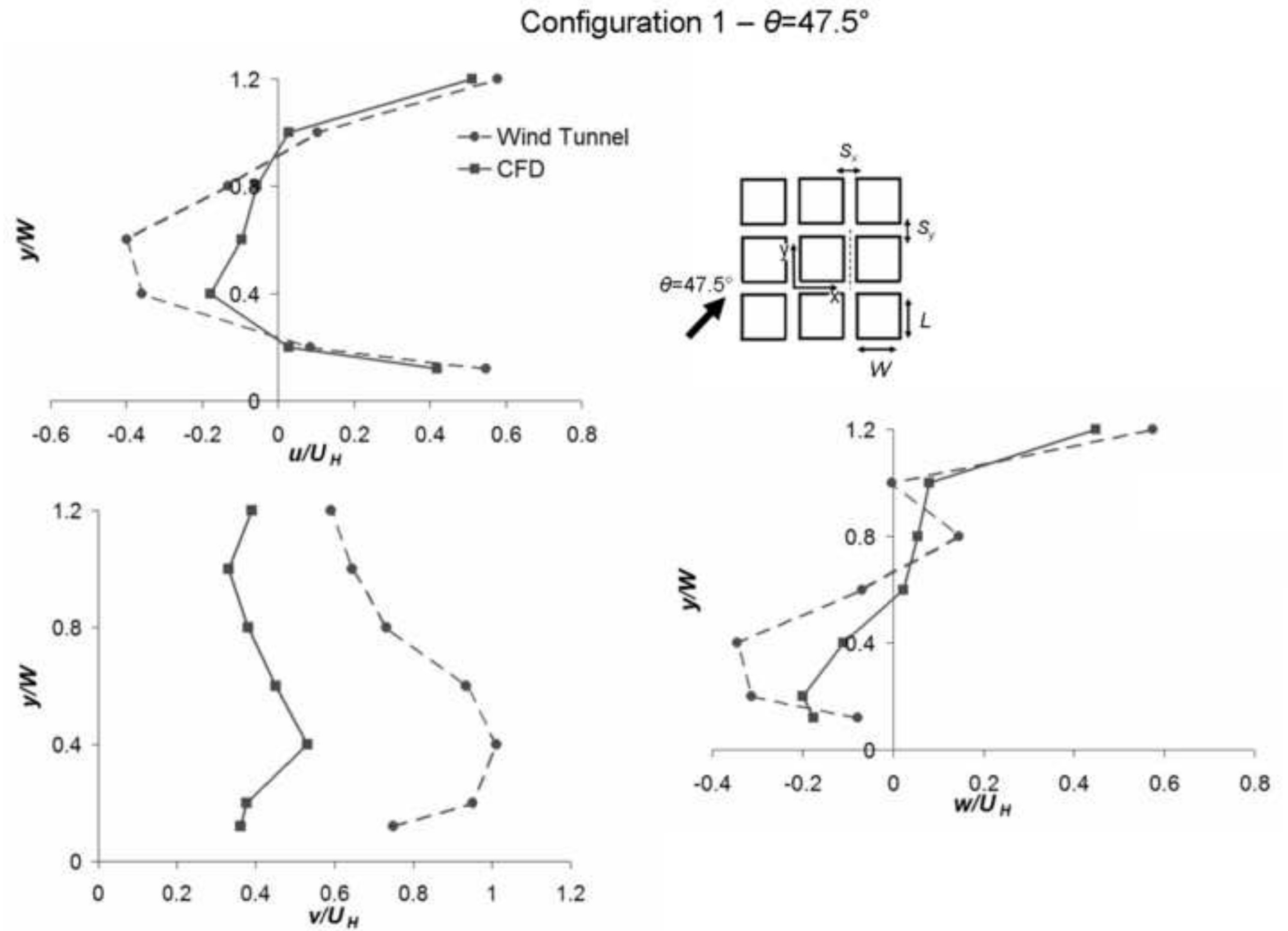
Configuration 1 – θ=47.5°
Wind Tunnel
CFD
y/W
u/U_H
v/U_H
w/U_H
θ=47.5°
S_x
S_y
L
W
x
y

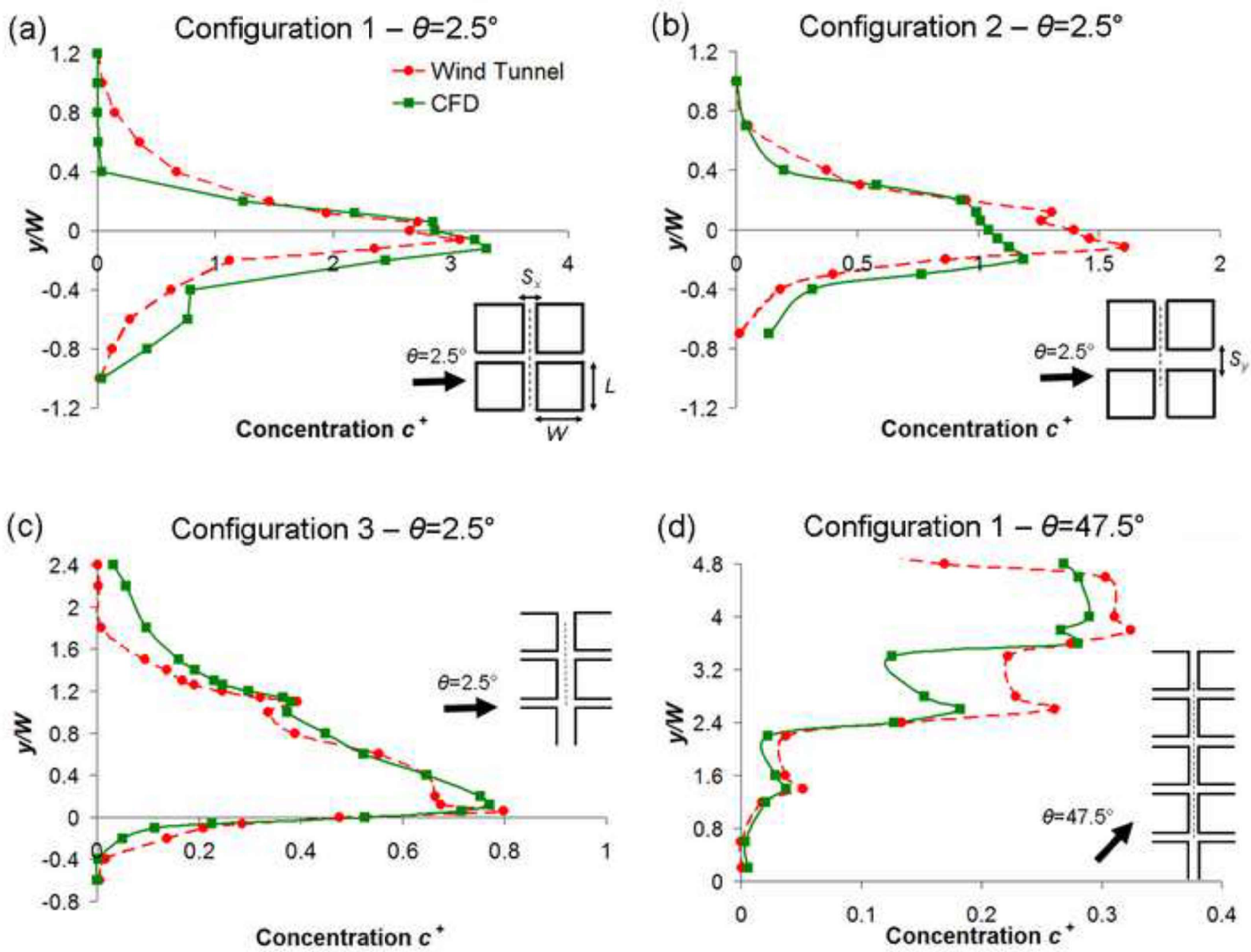
(a)
Configuration 1 – θ=2.5°
Wind Tunnel
CFD
y/W
Concentration c⁺
θ=2.5°
S_x
L
W
(b)
Configuration 2 – θ=2.5°
y/W
Concentration c⁺
θ=2.5°
S_y
(c)
Configuration 3 – θ=2.5°
y/W
Concentration c⁺
θ=2.5°
(d)
Configuration 1 – θ=47.5°
y/W
Concentration c⁺
θ=47.5°

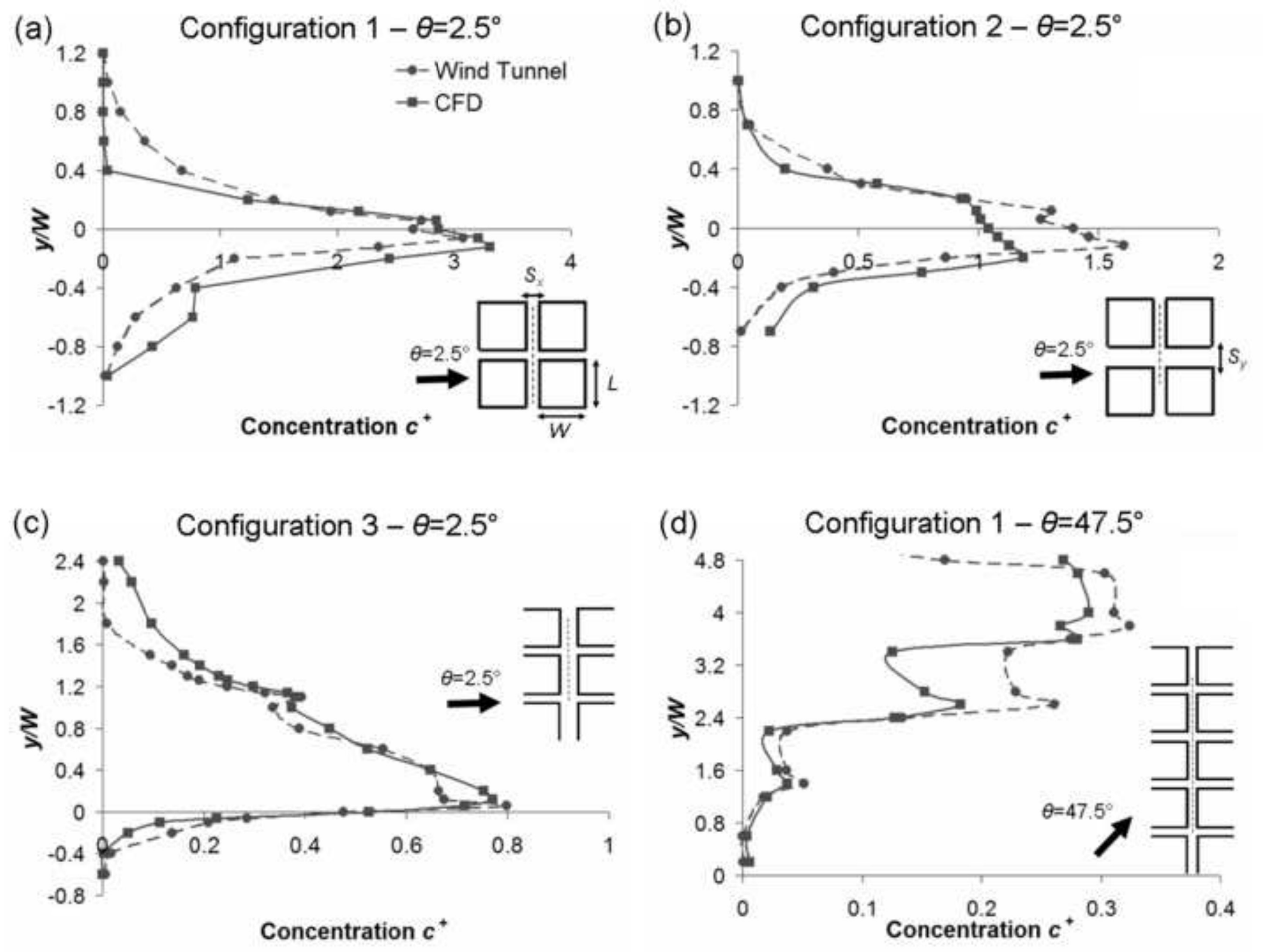
(a)
Configuration 1 – θ=2.5°
Wind Tunnel
CFD
y/W
Concentration c+
θ=2.5°
Sx
L
W
(b)
Configuration 2 – θ=2.5°
y/W
Concentration c+
θ=2.5°
Sy
(c)
Configuration 3 – θ=2.5°
y/W
Concentration c+
θ=2.5°
(d)
Configuration 1 – θ=47.5°
y/W
Concentration c+
θ=47.5°

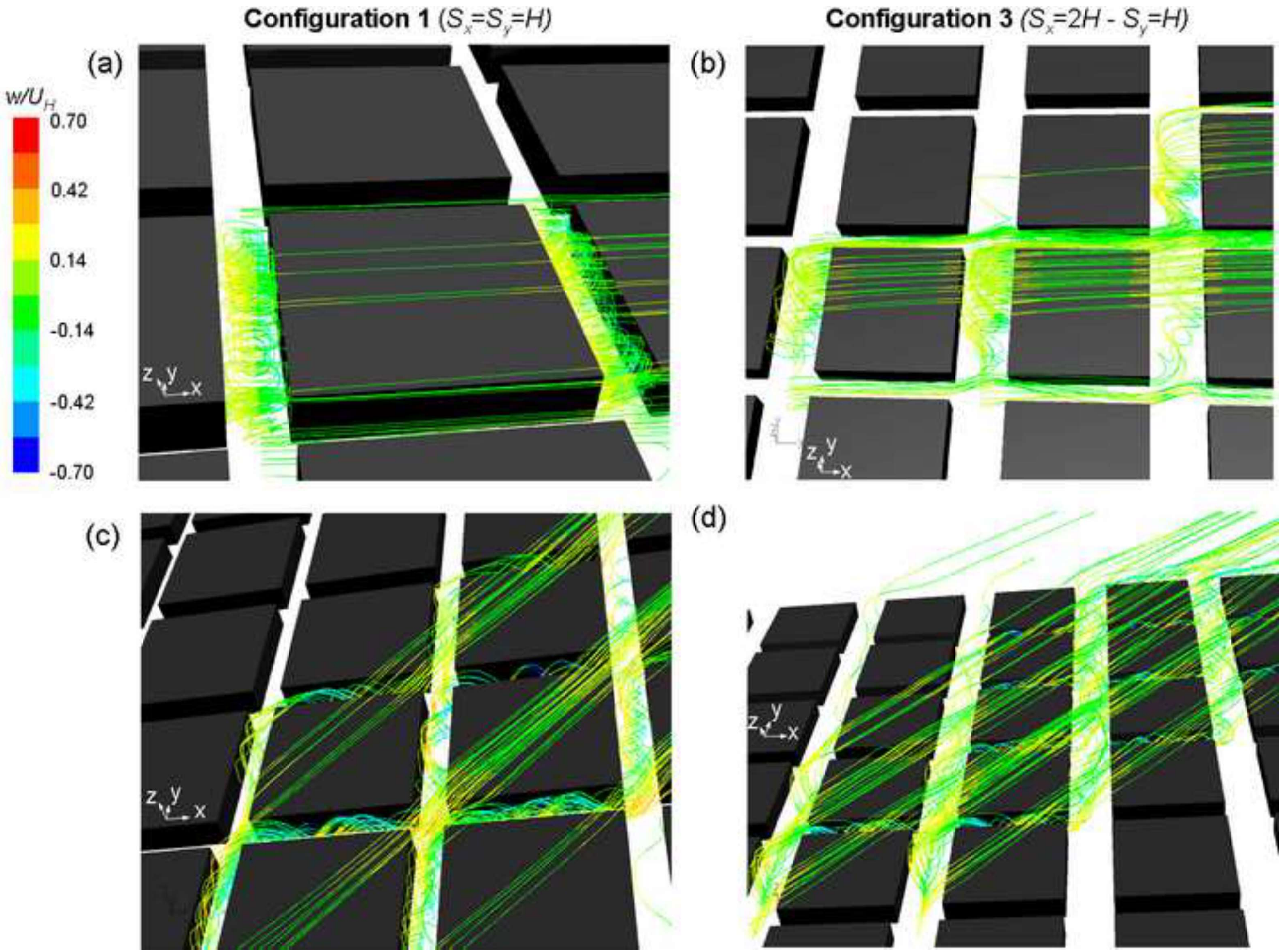
Configuration 1 (S_x=S_y=H)
Configuration 3 (S_x=2H - S_y=H)
(a)
(b)
(c)
(d)
w/U_H
0.70
0.42
0.14
-0.14
-0.42
-0.70
z y x

fig.8_bw_final.tif

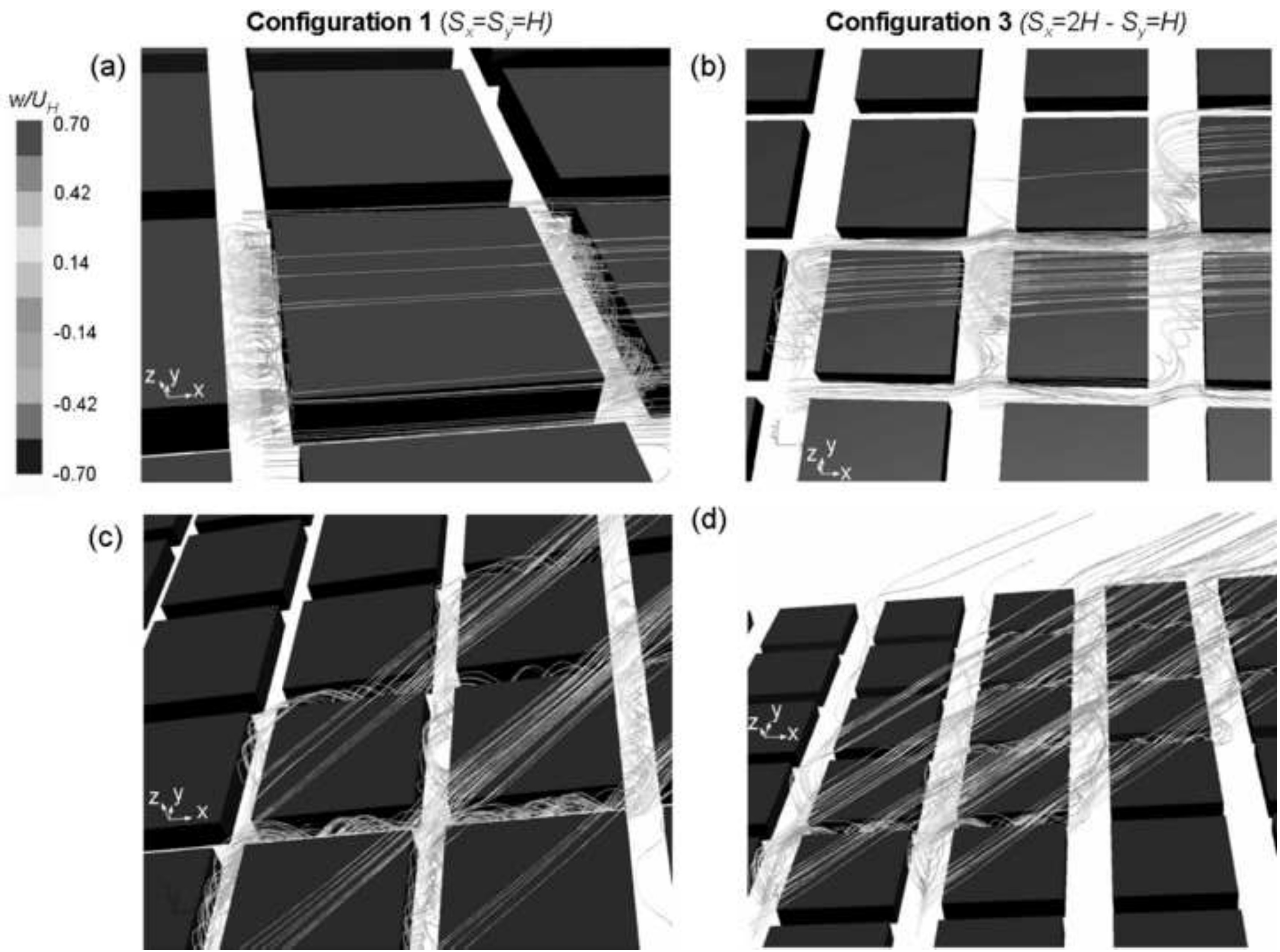

fig.9_final.tif

Click here to download high resolution image

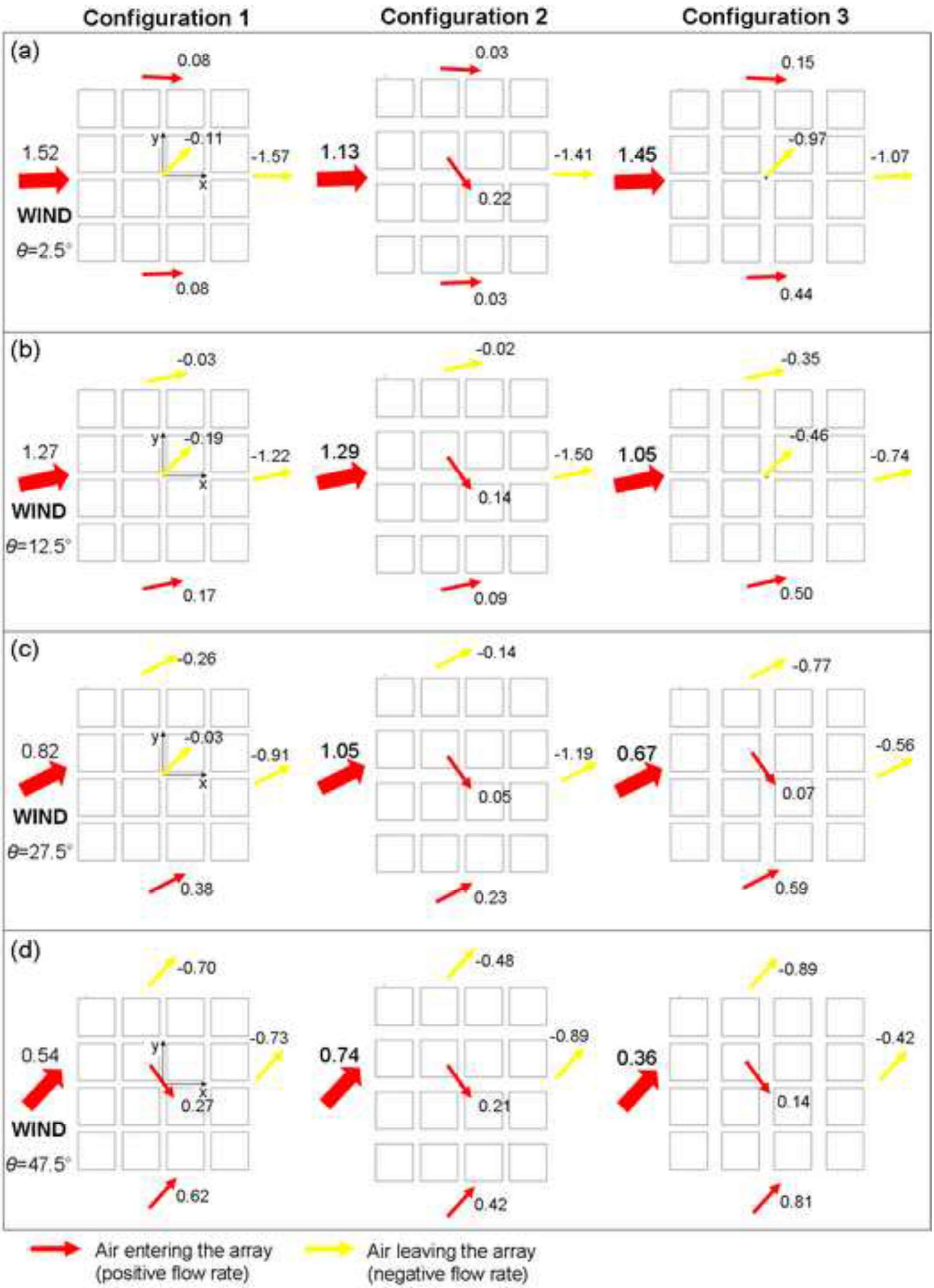

fig.9_bw_final.tif
Click here to download high resolution image

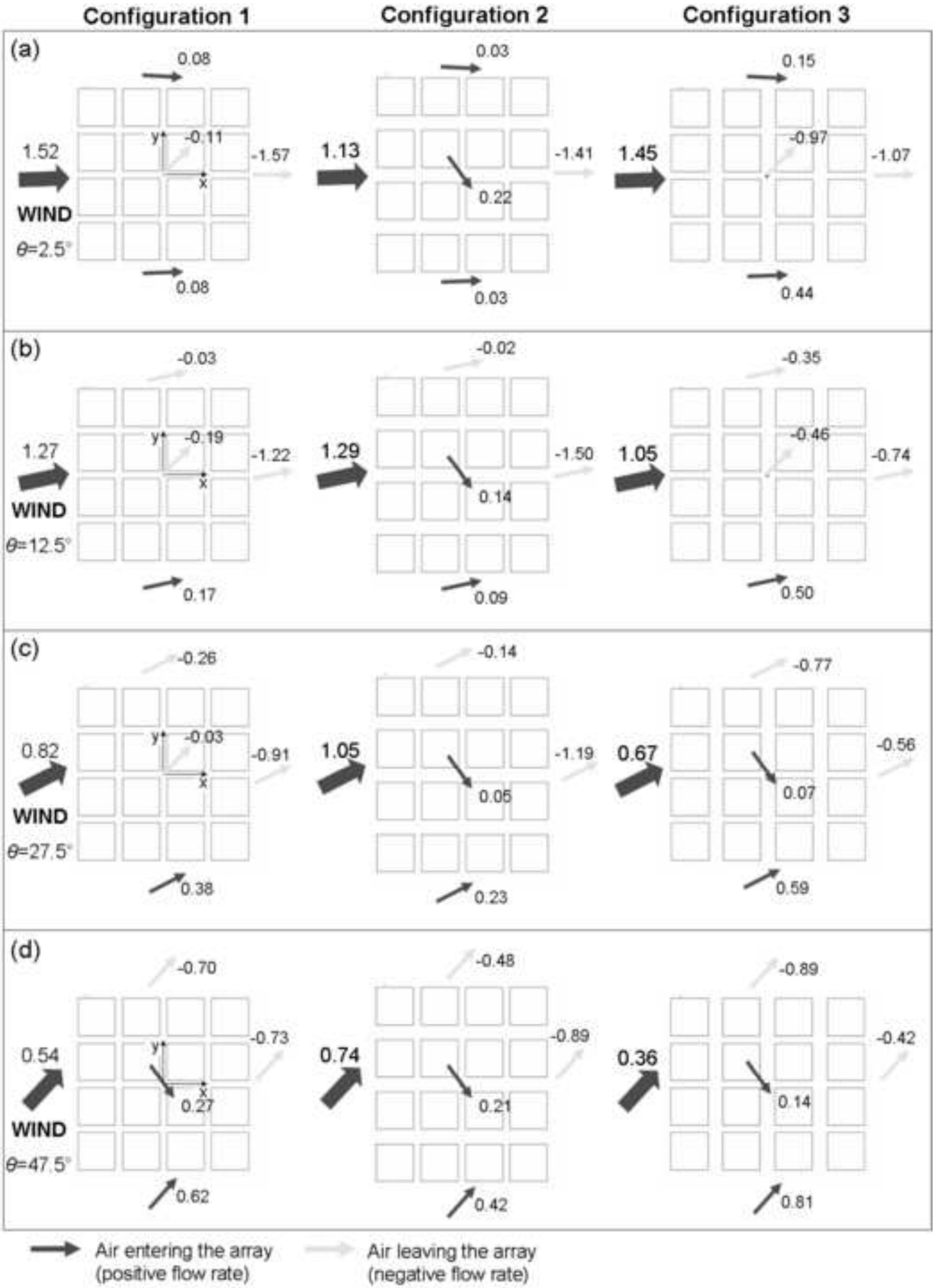

fig.10_final.tif
Click here to download high resolution image

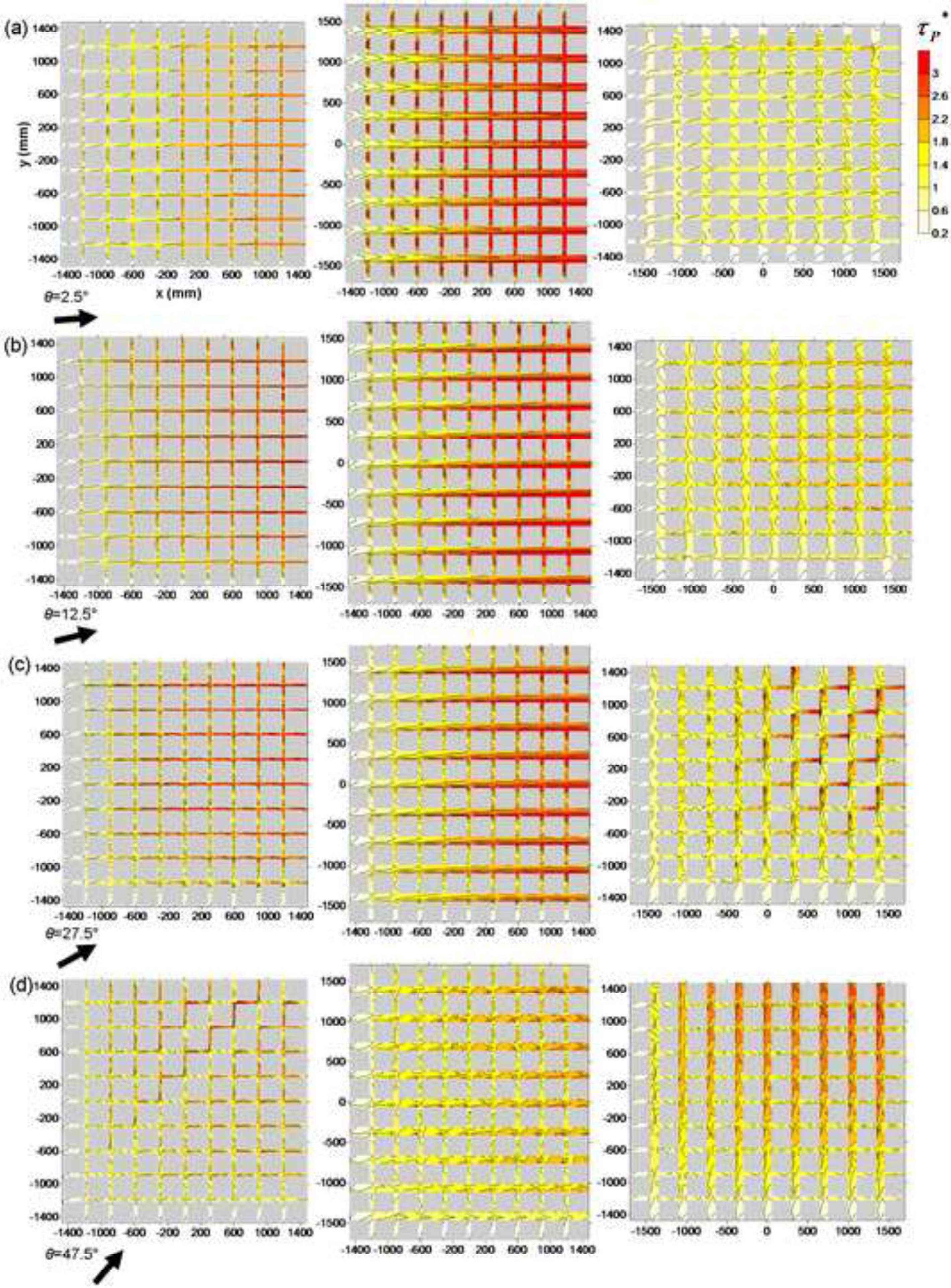

fig.10_bw_final.tif
Click here to download high resolution image

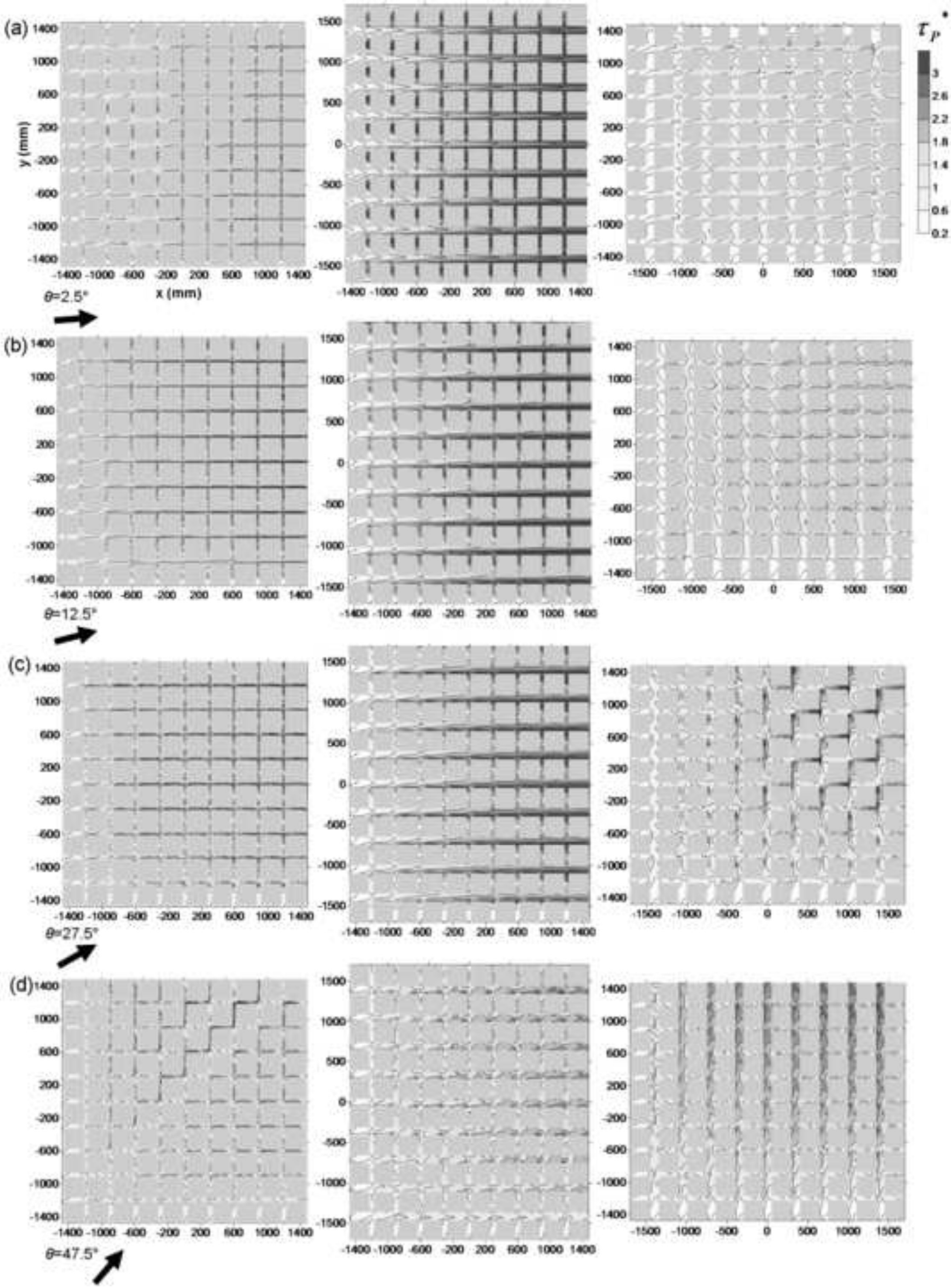

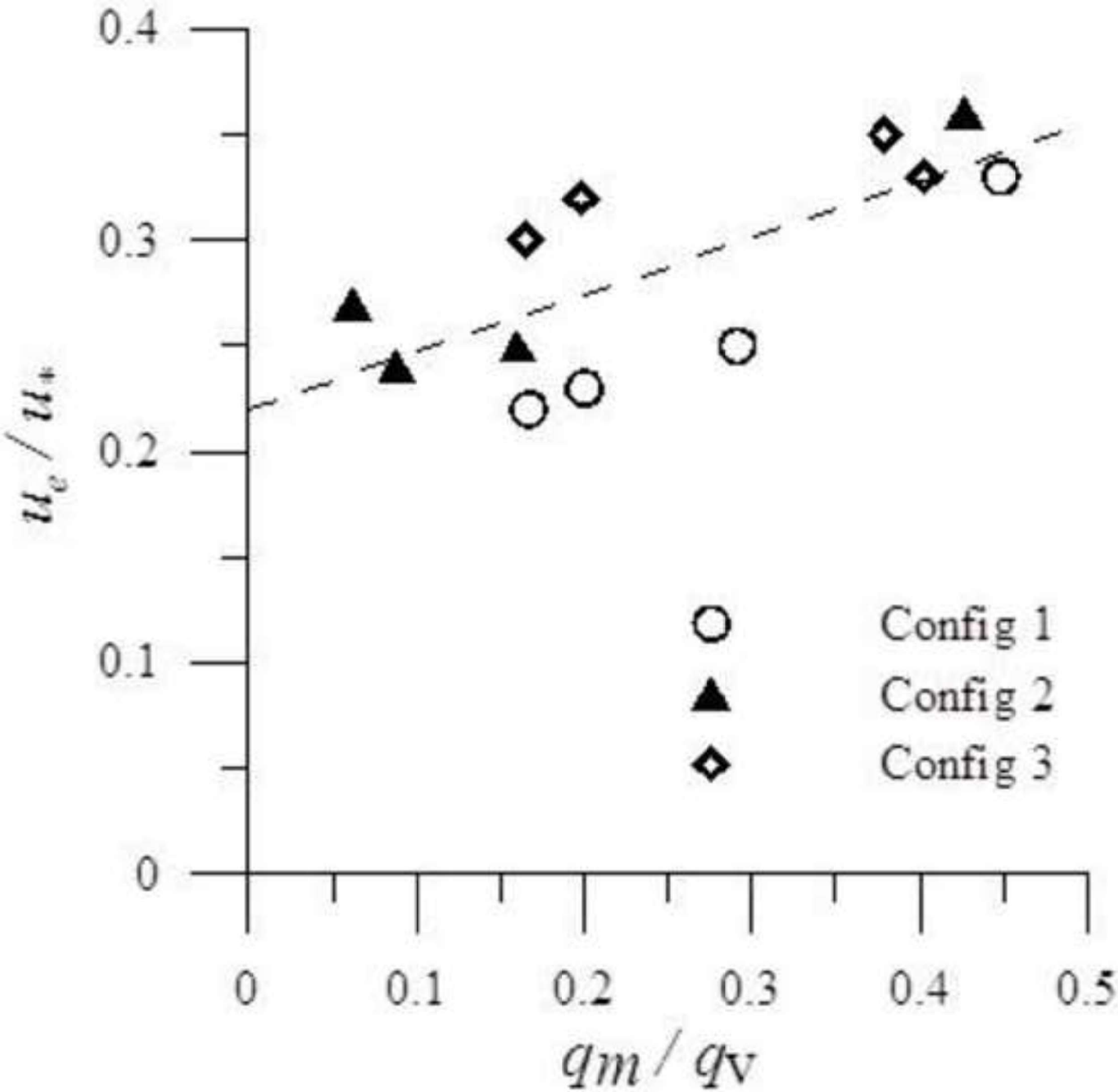
0.4
0.3
0.2
0.1
0
u_e / u_*
Config 1
Config 2
Config 3
0
0.1
0.2
0.3
0.4
0.5
qm / qv

Tables

Table 1
Values of the frontal index area (λ_f) for the study configurations.

	Configuration 1	Configurations 2 and 3
Wind direction θ=2.5°	0.14	0.12
θ=12.5°	0.17	0.14
θ=27.5°	0.19	0.16
θ=47.5°	0.20	0.17

Table 2
Results of the concentration statistical analysis. N/A stands for Not Available being wind tunnel data not available for that case.

		Configuration 1	Configuration 2	Configuration 3
NMSE	**Wind direction θ =2.5°**	0.22	0.54	1.08
	θ =47.5°	0.35	0.43	N/A
FAC2	**θ =2.5°**	0.54	0.74	0.71
	θ =47.5°	0.63	0.62	N/A
FB (FB_{fn}-FB_{fb})	**θ =2.5°**	0.08 (0.18-0.10)	0.22 (0.30-0.08)	0.11 (0.29-0.18)
	θ =47.5°	0.21 (0.30-0.09)	0.18 (0.31-0.13)	N/A
Hit Rate	**θ =2.5°**	0.54	0.53	0.56
	θ =47.5°	0.58	0.60	N/A

Table 3

Normalized mean age of air at pedestrian level.

		Configuration 1	Configuration 2	Configuration 3
Maximum	**Wind direction *θ=2.5°***	2.83	4.45	2.12
	θ=12.5°	3.54	4.07	2.56
	θ=27.5°	3.87	4.18	4.03
	θ=47.5°	3.80	3.36	3.58
Spatially-averaged	***θ=2.5°***	1.64	2.19	0.93
	θ=12.5°	1.88	1.95	1.00
	θ=27.5°	1.86	1.85	1.65
	θ=47.5°	1.50	1.38	1.31
Standard deviation	***θ=2.5°***	0.63	0.89	0.39
	θ=12.5°	0.71	0.81	0.65
	θ=27.5°	0.77	0.83	0.58
	θ=47.5°	0.63	0.52	0.65

Table 4

Dimensionless vertical exchange velocity u_e/u_*.

	Configuration 1	**Configuration 2**	**Configuration 3**
Wind direction *θ=2.5°*	0.23	0.27	0.32
θ=12.5°	0.22	0.24	0.30
θ=27.5°	0.25	0.25	0.35
θ=47.5°	0.33	0.36	0.33

Table 5

Ratio q_m/q_V (%) between the mean vertical mass flux and the total mass flux through the exchange surface A_{roof}.

q_m/q_V **(%)**	**Configuration 1**	**Configuration 2**	**Configuration 3**
Wind direction *θ=2.5°*	20.0	6.2	19.8
θ=12.5°	16.7	8.8	16.5
θ=27.5°	29.1	16.0	37.9
θ=47.5°	44.8	42.6	40.2